

CONFIDENTIAL

Copy 6
RM E54A20

NACA RM E54A20



RESEARCH MEMORANDUM

APPLICATION OF RADIAL-EQUILIBRIUM CONDITION TO AXIAL-FLOW
TURBOMACHINE DESIGN INCLUDING CONSIDERATION OF CHANGE
OF ENTROPY WITH RADIUS DOWNSTREAM OF BLADE ROW

By James E. Hatch, Charles C. Giamati, and Robert J. Jackson

Lewis Flight Propulsion Laboratory
Cleveland, Ohio
CLASSIFICATION CHANGED

To UNCLASSIFIED

By authority of NACA Reels + RN 124 Date effective Jan. 20, 1958
UAT 2-12-58

CLASSIFIED DOCUMENT

This material contains information affecting the National Defense of the United States within the meaning of the espionage laws, Title 18, U.S.C., Secs. 793 and 794, the transmission or revelation of which in any manner to an unauthorized person is prohibited by law.

**NATIONAL ADVISORY COMMITTEE
FOR AERONAUTICS LIBRARY COPY**

WASHINGTON
April 14, 1954
APR 16 1954

Lewis Flight Propulsion Laboratory
Langley Field, Virginia

CONFIDENTIAL



NATIONAL ADVISORY COMMITTEE FOR AERONAUTICS

RESEARCH MEMORANDUM

APPLICATION OF RADIAL-EQUILIBRIUM CONDITION TO AXIAL-FLOW TURBOMACHINE

DESIGN INCLUDING CONSIDERATION OF CHANGE OF ENTROPY

WITH RADIUS DOWNSTREAM OF BLADE ROW

By James E. Hatch, Charles C. Giamati, and Robert J. Jackson

SUMMARY


3038

CA-1

An investigation was made of the validity of application of the simplified-radial-equilibrium equation to axial-flow turbomachines. Two types of calculations based on the assumption of simplified radial equilibrium were made of radial distributions of axial velocities for comparisons with data from several compressor configurations. One type of calculation incorporated the measured radial variation of stagnation-pressure losses by means of a term in the radial-equilibrium equation expressing the radial variation of entropy. The second type of calculation did not include this term.

In order to compute accurately the radial variation of velocities, it was necessary in general to include the measured stagnation-pressure losses in the simplified-radial-equilibrium equation. The assumption of zero radial gradient of entropy was invalid for the calculation of velocities at axial stations more than one or two blade rows downstream from a region of uniform entropy. At an axial station following several stages of a multistage compressor, large discrepancies were observed between measured velocities and velocities computed from the simplified-radial-equilibrium calculation which neglected the entropy term, while the incorporation of the entropy term led to calculated velocities which agreed closely with data.

Very close agreement was observed between the velocities calculated by using an entropy gradient and measured velocities in the boundary-layer regions at the hub and tip while the second type of calculation, with the entropy gradient neglected, was not correct. This trend suggests that the blockage effect of the boundary layer can be taken into account by a design assumption of the boundary-layer stagnation-pressure profile based upon available boundary-layer loss data.



A velocity-diagram design method, based upon the results of this investigation and including the effect of the estimated stagnation pressures on the design axial-velocity profile, is suggested in this report.

INTRODUCTION

The design procedure currently in use for a multistage axial-flow compressor is divided into two phases, the first of which is concerned with the determination of stage velocity diagrams for the inlet and outlet to the various blade rows, while the second is concerned with the selection of blade shapes which will yield these diagrams. In the first phase the radial-equilibrium condition (the radial component of the equation of motion) is used. This condition specifies the radial pressure gradient that is necessary to provide the centripetal force to maintain a curved flow path (refs. 1 to 3) through the compressor.

In design work a form of the radial-equilibrium condition which has been used is given in reference 1 (eq. (14)) as (in the terminology of this report)

$$\frac{\partial H}{\partial r} = F_r + t \frac{\partial s}{\partial r} + \frac{V_\theta}{r} \frac{\partial(rV_\theta)}{\partial r} + V_z \frac{\partial V_z}{\partial r} - V_z \frac{\partial V_r}{\partial z} \quad (1)$$

This equation was derived under the assumption of axially symmetric flow in a fluid of negligible viscosity. When the equation is applied to an axial station at the inlet or outlet of a blade row, the blade-force term represented by F_r is zero.

In reference 1, the effect of the radial-flow term $\left(-V_z \frac{\partial V_r}{\partial z}\right)$ of equation (1) on the radial distribution of the state of the gas was investigated. This was done for nonviscous-flow problems by comparing solutions obtained by applying equation (1) with solutions obtained by applying a modification of equation (1) (the simplified-radial-equilibrium approximation) which dropped the radial-flow term. For the purposes of this analysis, the entropy term $\left(t \frac{\partial s}{\partial r}\right)$ of equation (1) was neglected in these solutions because of the assumptions of nonviscous flow and no heat transfer.

These methods for inviscid fluids do not account for the radial variation of total-pressure losses which occur across a blade row in a compressor. In order to include these losses in the velocity-diagram calculations, the radial variation in total-pressure loss can be related to the radial variation in entropy and as such included in the radial-equilibrium calculations. A method of velocity-diagram calculation which includes the entropy term is shown in this report. In order to ascertain

the effect of the entropy term of equation (1) on the radial distribution of the state of the gas, velocities are computed by using a modification of equation (1) which includes the entropy term but drops the radial-flow term (simplified radial equilibrium including entropy gradient) and are compared with velocities computed from a modification of equation (1) which does not include the entropy term and also drops the radial-flow term (simplified-radial-equilibrium approximation). These velocity distributions, which are computed for several compressor configurations, are compared in each case with measured velocities to see if it is possible to predict correctly the stage-velocity diagrams by including the entropy term in the calculations.

The development of the solution including entropy gradient to the radial-equilibrium equation is presented in the section ANALYSIS OF EQUATIONS. The differences in the assumptions used for this solution and for the solutions obtained in reference 1 are discussed, and the significance of the entropy term in the radial-equilibrium solution is pointed out.

The methods used to adapt the analytical solutions (simplified radial equilibrium including entropy gradient and simplified-radial-equilibrium approximation) to measured data are shown in the section ANALYSIS OF EXPERIMENTAL DATA. The experimental data are taken from configurations described in references 4 to 10. In most cases the data were available only in the "main-stream region"; however, in two configurations, data obtained near the end walls of the compressors were used to see if the axial-velocity profiles in the boundary layer could be accounted for by the solution based on simplified radial equilibrium including an entropy gradient. The remainder of the data in the section ANALYSIS OF EXPERIMENTAL DATA is grouped as single-stage data or data from middle or end stages of a multistage compressor.

The section entitled ANALYSIS OF DESIGN TECHNIQUE suggests possible uses of the approximation of simplified radial equilibrium including an entropy gradient in a design procedure. An example of a fixed-area velocity-diagram calculation is outlined in detail.

SYMBOLS

The following symbols are used in this report:

- c_p specific heat at constant pressure, ft-lb/(slug)(°R), equal to Jgc_p engineering units
- D diffusion factor (ref. 11)
- F blade force, lb/slug

| | |
|----------------|---|
| g | acceleration due to gravity, ft/sec ² |
| H | total enthalpy, ft-lb/slug, equal to JgH engineering units |
| J | mechanical equivalent of heat, ft-lb/Btu |
| K | curvature of path, reciprocal of radius of curvature, ft ⁻¹ |
| P | total pressure, lb/sq ft |
| p | static pressure, lb/sq ft |
| R | gas constant, ft-lb/(slug)(°R), equal to gR engineering units |
| r | radius, ft |
| s | entropy, ft-lb/(slug)(°R), equal to gs engineering units |
| T | total temperature, °R |
| t | static temperature, °R |
| U | rotor velocity, ft/sec |
| V | gas velocity, ft/sec |
| V _u | absolute gas velocity at station where some variables are unknown, ft/sec |
| W | weight flow, lb/sec |
| z | axial distance, ft |
| β | absolute air angle, angle between air velocity and axial direction, deg |
| γ | ratio of specific heats |
| θ | angular coordinate, deg |
| ρ | static density, slugs/cu ft |
| φ | stage-inlet-flow coefficient, $(V_z/U_t)_{av}$ |

Subscripts:

| | |
|----|---------|
| av | average |
| h | hub |

| | |
|-------------|---|
| k | radial station where variables are known |
| m | mean |
| r | radial direction |
| ref | reference |
| t | tip |
| u | radial station where some variables are unknown |
| z | axial direction |
| θ | tangential direction |
| O | pipe inlet or compressor depression tank |
| 1,2,3,... n | axial station downstream of n th blade row, where the guide vanes are the first blade row. |

ANALYSIS OF EQUATIONS

Assumptions

The behavior of a fluid in a compressor can be investigated by applying the conservation laws of matter, momentum, and energy to the flow. The assumptions of axial symmetry and negligible viscosity are reasonable conditions to specify in order to investigate this flow. Using these assumptions, the authors of reference 1 developed the following form of the combined momentum and energy equations for a cylindrical coordinate system, where r , z , and θ are independent variables:

$$\frac{\partial H}{\partial r} = F_r + t \frac{\partial s}{\partial r} + \frac{v_\theta}{r} \frac{\partial(rv_\theta)}{\partial r} + v_z \frac{\partial v_z}{\partial r} - v_z \frac{\partial v_r}{\partial z} \quad (2a)$$

$$0 = F_\theta - \frac{1}{r} \left[v_r \frac{\partial(rv_\theta)}{\partial r} + v_z \frac{\partial(rv_\theta)}{\partial z} \right] \quad (2b)$$

$$\frac{\partial H}{\partial z} = F_z + t \frac{\partial s}{\partial z} + \frac{v_\theta}{r} \frac{\partial(rv_\theta)}{\partial z} - v_r \frac{\partial v_z}{\partial r} + v_r \frac{\partial v_r}{\partial z} \quad (2c)$$

In applying these equations (eqs. (14), (15), and (16) of ref. 1 in the terminology of this report), the fluid was considered to be inviscid throughout the compressor so that the variation in entropy could be caused only by heat transfer. Thus, the entropy term was neglected in

the solutions presented since no heat transfer was assumed. However, in a real compressor, viscous flows exist and a radial variation of blade-row total-pressure losses, which gives rise to a radial entropy gradient, can occur as the viscous fluid passes through the blade rows where large velocity gradients and large wetted surface areas are present.

The effect on axial-velocity profiles of viscous forces which occur in the space between blade rows is small compared with the effect on the axial-velocity profiles of losses which have occurred upstream through the blade rows. Thus when the flow in the space between blade rows is examined, the fluid is considered to be inviscid (hence eqs. (2) are applicable) with a radial entropy gradient at the point of interest. The inclusion of the entropy term in applying the radial-equilibrium condition may be regarded as a loss correction included in the equations for inviscid flow. In this investigation, an experimental evaluation of the losses is included in the analytical solutions.

An example of how these concepts can be applied to the simple case of pipe flow is shown in the following section. The manner in which the equations are applied is analogous to the manner in which they are applied to actual compressors for this investigation.

Significance of Entropy Gradient

For application to pipe flow or to the space between blade rows of a compressor, equations (2) are more conveniently written as

$$c_p \frac{\partial T}{\partial r} = t \frac{\partial s}{\partial r} + V_\theta \frac{\partial V_\theta}{\partial r} + \frac{V_\theta^2}{r} + V_z \frac{\partial V_z}{\partial r} - V_z \frac{\partial V_r}{\partial z} \quad (3a)$$

$$0 = V_r \frac{\partial V_\theta}{\partial r} + \frac{V_r V_\theta}{r} + V_z \frac{\partial V_\theta}{\partial z} \quad (3b)$$

$$c_p \frac{\partial T}{\partial z} = t \frac{\partial s}{\partial z} + V_r \frac{\partial V_r}{\partial z} + V_\theta \frac{\partial V_\theta}{\partial z} - V_r \frac{\partial V_z}{\partial r} \quad (3c)$$

In the case of pipe flow, T is a constant throughout the flow and is equal to T_0 , and $V_\theta = V_r = 0$. In order to apply equations (3) to an axial station downstream of the inlet, the fluid must be considered inviscid at this station. This condition, along with $V_\theta = V_r = 0$, reduces the set of equations (3) to

$$0 = t \frac{\partial s}{\partial r} + V_z \frac{\partial V_z}{\partial r} \quad (4)$$

An assumption that $\partial s / \partial r = 0$ leads to the conclusion that $V_z = \text{constant}$ along the radius. This conclusion is invalid near the pipe walls due to the previous viscous flow upstream. The nonvanishing radial gradient of entropy can be introduced in terms of total pressure and temperature. By the definition of stagnation conditions, stagnation entropy equals static entropy and is a function of stagnation pressure and temperature as follows:

$$s = s_{\text{ref}} + R \ln \left[\frac{(T/T_{\text{ref}})^{\frac{\gamma}{\gamma-1}}}{P/P_{\text{ref}}} \right] \quad (5)$$

For this case, the reference point is the pipe inlet and $T = T_{\text{ref}} = T_0$. Equation (5) reduces to $s = s_0 + R(\ln P_0) - R(\ln P)$, which then yields $\partial s / \partial r = -R \partial(\ln P) / \partial r$, since entropy and total pressures are constant with radius at the pipe inlet. When both sides of this last equation are multiplied by t and the result is substituted in equation (4), the equation becomes

$$\frac{\partial}{\partial r} \frac{v^2}{2} = R \left(T - \frac{v^2}{2c_p} \right) \frac{\partial}{\partial r} (\ln P)$$

Integration of this equation from r_m to r gives

$$\ln \left(\frac{T - \frac{v^2}{2c_p}}{T - \frac{v_m^2}{2c_p}} \right) = \ln \left[\left(\frac{P_m}{P} \right)^{\frac{\gamma-1}{\gamma}} \right]$$

or

$$T - \frac{v^2}{2c_p} = \left(T - \frac{v_m^2}{2c_p} \right) \left(\frac{P_m}{P} \right)^{\frac{\gamma-1}{\gamma}}$$

In terms of total enthalpy, this last equation becomes

$$v^2 = 2H - (2H - v_m^2) \left(\frac{P_m}{P} \right)^{\frac{\gamma-1}{\gamma}} \quad (6)$$

Since the whirl and radial accelerations are zero, static pressure is constant and does not appear in equation (6). For a given stagnation temperature, velocity is a function only of stagnation pressure. The reduction of stagnation pressure by viscous forces is associated with a reduction in velocity, and this relation is given by equation (6). The total-pressure losses near the pipe walls are reflected in the drop in

velocity in these regions; hence, the axial-velocity gradients agree qualitatively with the axial-velocity gradients predicted from viscous-flow equations. This example shows that in the case of pipe flow the stagnation-pressure-loss correction used in the radial component of an equation of motion for inviscid fluid can lead to results which are qualitatively correct for viscous fluids. Thus an analogous treatment of the more complicated problem of viscous flow through a compressor may be useful.

Significance of Radial-Flow Term

In order to discuss the effect of the radial-flow term on the radial variations of the state of the fluid, the term can be expanded into an expression involving the radius of curvature of the streamline in the r, z surface. When the differentiation along the streamline is considered,

$$V_z \frac{\partial V_r}{\partial z} = V_z \frac{\partial}{\partial z} \left(V_z \frac{\partial r}{\partial z} \right) = V_z \frac{\partial V_z}{\partial z} \frac{\partial r}{\partial z} + V_z^2 \frac{\partial^2 r}{\partial z^2}$$

Since

$$K = \frac{\frac{\partial^2 r}{\partial z^2}}{\left[1 + \left(\frac{\partial r}{\partial z} \right)^2 \right]^{3/2}}$$

where K is the curvature in the r, z plane or reciprocal of the radius of curvature, then

$$V_z \frac{\partial V_r}{\partial z} = V_r \frac{\partial V_z}{\partial z} + K V_z^2 \left[1 + \left(\frac{\partial r}{\partial z} \right)^2 \right]^{3/2} \quad (7)$$

From equation (7), the term $V_z \frac{\partial V_r}{\partial z}$ is affected both by the axial variation of axial velocity (as determined by the continuity condition) and the curvature of the streamlines. For the configurations considered in this report, the maximum hub taper is about 10° . Both the radial velocity and the axial variation of axial velocity at the measuring station in the space between blade rows are therefore small, and the first term of equation (7) can be neglected. The term $V_z \frac{\partial V_r}{\partial z}$, designated the radial-flow term, will be discussed in this report in terms of streamline curvature only. For compressors with large hub taper, such as transonic compressors designed for high pressure ratios, and with hub-tip radius ratios less than 0.5, the contribution to the radial-flow term by $V_r \frac{\partial V_z}{\partial z}$ may be significant. The formula for the curvature K shows that

the sign of the radial-flow term is positive for streamlines concave looking from the compressor casing (fig. 1) and negative for streamlines convex looking from the casing.

In the conventional tests of an axial-flow compressor, the instrumentation is not designed to determine the radial component of the absolute velocity after the blade rows since it is assumed to be small. This assumption is

$$V_{\theta}^2 + V_z^2 \cong V^2 \quad (8)$$

In this presentation, the radial-flow term which was included in reference 1 will be neglected. A solution which uses the entropy term will be obtained and compared with actual data. Within the limits of the assumptions of axial symmetry and negligible viscosity at this axial station, the difference between this solution and actual data may be attributed to the effect of neglecting the radial-flow term. A solution will also be obtained in which both the entropy term and the radial-flow term are neglected. The difference between this last solution (the simplified-radial-equilibrium approximation) and data may be attributed both to effects of radial entropy variation and the radial-flow term, again with the assumption that deviations from axial symmetry and negligible viscosity do not mask these effects. Consequently, a comparison of these two types of analytical solutions with compressor data may indicate the relative magnitude of the effect of radial entropy gradient and radial-flow term on the radial variations of the fluid state.

The type of flow distribution (radial variation of whirl) and the compressor geometry determine the importance of the radial-flow term. For free-vortex flow, little radial shift of streamlines occurs through blade rows so the radial-flow term is probably unimportant. The radial pressure gradients attendant to wheel-type or wheel-minus-vortex (symmetrical velocity diagram) distributions of whirl cause radial flows and appreciable curvature of the streamlines. This effect is discussed in reference 12 and tends to make the radial-flow term more important. The geometric characteristics of low hub-tip radius ratio, high hub curvature, and high aspect ratio tend to increase the importance of the radial-flow term.

ANALYSIS OF EXPERIMENTAL DATA

Application of Radial-Equilibrium Equation

In order to compare experimental data with the solutions based on simplified radial equilibrium including an entropy gradient and solutions based on simplified-radial-equilibrium approximation, equation 3(a) must

be solved and written in a form suited to convenient application to the data. By making several simplifying assumptions, a useful numerical solution of equation (3a) can be obtained.

When equation (3a) is integrated between a radius at which all the dependent variables are known or assumed (subscript k) and a radius at which some of the dependent variables are unknown (subscript u), a rearrangement (the radial-flow term is dropped) gives

$$V_{\theta,u}^2 + V_{z,u}^2 = 2R \int_{r_u}^{r_k} t \frac{\partial(s/R)}{\partial r} dr + V_{\theta,k}^2 + V_{z,k}^2 + 2 \int_{r_u}^{r_k} \frac{V_{\theta}^2}{r} dr + 2c_p(T_u - T_k) \quad (9)$$

It is desirable for comparing analytical results with actual data to put equation (9) into a form involving only absolute velocity, absolute air angle, total pressure, and total temperature after the blade row. This expression can be developed as follows:

By using equation (8) and the steady-flow energy equation

$$t = T - V^2/2c_p \quad (10)$$

equation (9) can be written as

$$V_u^2 = \int_{r_u}^{r_k} (2RT - \frac{\gamma-1}{\gamma} V^2) \frac{\partial(s/R)}{\partial r} dr + V_k^2 + 2 \int_{r_u}^{r_k} \frac{V_{\theta}^2}{r} dr + 2c_p(T_u - T_k) \quad (11)$$

A numerical solution of equation (11) for V_u may be obtained if the following simplifying assumptions are made in order to facilitate integration of equation (11):

- (1) V_{θ}^2/r varies linearly between the two radii of integration.
- (2) T varies linearly between the two radii of integration.
- (3) V^2 varies linearly between the two radii of integration.
- (4) s/R varies linearly between the two radii of integration.

These four assumptions are nearly correct if the radial positions are close together. After the flow problem has been solved, the above

integrands can be plotted against the variable of integration to check these assumptions of linearity, and corrections can be made if necessary until equation (11) is satisfied.

With the use of the assumption of linear variation of T and V^2 between the radii of integration, the first integral on the right side of equation (11) may be evaluated by the trapezoidal rule as follows:

$$\int_{r_u}^{r_k} \left(2RT - \frac{\gamma-1}{\gamma} V^2 \right) \frac{\partial(s/R)}{\partial r} dr = \left[R(T_k + T_u) - \frac{\gamma-1}{2\gamma} (V_k^2 + V_u^2) \right] \left(\frac{s_k}{R} - \frac{s_u}{R} \right)$$

The entropy at a fixed radial position at axial station 2, for example, may be expressed (from eq. (5)) as

$$\frac{s_2}{R} = \frac{s_{ref}}{R} + \ln \left[\frac{(T_2/T_{ref})^{\frac{\gamma}{\gamma-1}}}{P_2/P_{ref}} \right] \quad (5a)$$

where s_{ref} is the entropy of the gas at some reference point upstream.

For the data presented herein, the reference point is the depression tank and $s_{ref} = s_0$. Therefore, at axial station 2 the quantity

$s_{2,k}/R - s_{2,u}/R$ can be evaluated as follows:

$$\frac{s_{2,k}}{R} - \frac{s_{2,u}}{R} = \ln \left[\frac{(T_{2,k})^{\frac{\gamma}{\gamma-1}} / P_{2,k}}{T_0 / P_0} \right] - \ln \left[\frac{(T_{2,u})^{\frac{\gamma}{\gamma-1}} / P_{2,u}}{T_0 / P_0} \right]$$

The third term on the right side of equation (11) is also evaluated by the trapezoidal rule, and with the relation $V_\theta = V \sin \beta$ this term can be written

$$2 \int_{r_u}^{r_k} \frac{V^2 \sin^2 \beta}{r} dr = \left(\frac{V_k^2 \sin^2 \beta_k}{r_k} + \frac{V_u^2 \sin^2 \beta_u}{r_u} \right) (r_k - r_u)$$

After the integrals have been evaluated in equation (11), the resulting form may be solved for V_u :

$$V_u = \sqrt{\frac{V_k^2 \left[1 + \left(1 - \frac{r_u}{r_k} \right) \sin^2 \beta_k \right] + 2c_p(T_u - T_k) + \frac{\gamma-1}{\gamma} \left(\frac{s_k}{R} - \frac{s_u}{R} \right) \left[c_p(T_k + T_u) - \frac{V_k^2}{2} \right]}{1 - \left(\frac{r_k}{r_u} - 1 \right) \sin^2 \beta_u + \frac{\gamma-1}{2\gamma} \left(\frac{s_k}{R} - \frac{s_u}{R} \right)} \quad (12)$$

Equation (12) gives the solution for simplified radial equilibrium including an entropy gradient. A solution for the simplified-radial-equilibrium approximation is obtained by keeping the entropy constant radially (i.e., the term $s_k/R - s_u/R$ equal to zero) in equation (12). It should be noted that c_p and R must have units of (ft-lb)/(slug ($^{\circ}R$)) in this derivation.

Solution of Velocity Distributions

The solution for velocity at all radii based on simplified radial equilibrium including entropy gradient requires a knowledge of the radial variations of total pressure, total temperature, and absolute air angle after the blade row, and the inlet conditions to the compressor. With the aid of the absolute measured velocity at or near the mean radius as the initial V_k , solutions of equation (12) for V_u for the radial position on either side of the mean radius can be obtained. These values of V_u are then taken as V_k for the solution of velocity at the next radial position nearer the hub and tip. When this first velocity distribution has been calculated across the passage, the weight flow is computed by using the relation

$$W = 2\pi g \int_{r_h}^{r_t} \rho V_z r dr \quad (13)$$

when the static density is given by

$$\rho = \frac{P}{RT} \left(1 - \frac{r-1}{r} \frac{V^2}{2RT} \right)^{\frac{1}{r-1}} \quad (14)$$

The value of weight flow obtained from equation (13) is compared with the weight flow calculated from the radial-survey data, and the initial value of V_k at the mean radius is corrected by the ratio of these weight flows to give a second value of V_k at the mean radius for the second approximation. This process is repeated until continuity is satisfied as evidenced by the agreement of the actual and computed weight flows.

The same procedure is used to compute the values of V_u from the simplified-radial-equilibrium approximation. As stated previously in the section Application of Radial-Equilibrium Equation, the term $(s_k - s_u)/R$ is set equal to zero in equation (12), which then reduces to the simplified-radial-equilibrium approximation.

PRESENTATION OF EXPERIMENTAL DATA

Interpretation of Data

3038

Comparisons were made among the measured and two types of computed velocities for the portion of the flow outside the boundary layer after guide vanes, rotors, and stators for a variety of compressor configurations. The blade rows involved cover a wide range of aspect ratio and hub-tip radius ratio. The comparison also covers a range of operating conditions for the blade row so that the effect of varying losses upon the relative magnitude of the terms of the equilibrium equation may be investigated. In this presentation the discussion is divided into two sections.

The first section presents results for stages with uniform entropy at the inlet (single stages and inlet stages of multistage compressors); the second section presents results for stages with an inlet entropy gradient (middle and end stages of a multistage unit). This division is made because it is expected that the effect of the entropy gradient will be markedly greater for stages with an inlet entropy gradient than for stages with uniform inlet entropy. These sections are subdivided for convenience into subsections for comparisons of velocities after rotors and stators. Most of these measurements were taken in the free-stream region out of the end-wall boundary layers. However, a limited amount of boundary-layer data was obtained and is discussed in a further subdivision entitled "Boundary-layer data" of the section on inlet stages. A large number of calculations were made for each configuration, but only representative results are presented in this report.

In order to clarify the method of comparing velocities, figure 2 shows the effect of adding the entropy-gradient term to the simplified-radial-equilibrium approximations. It can be seen, in figure 2(b) for instance, that using the loss term not only reduces the velocities at certain radii but also shifts the profile vertically to satisfy continuity. The effects of loss profile with minimum losses at points other than the hub, mean, or tip radius could be similarly analyzed.

After the solution with simplified radial equilibrium including an entropy gradient for velocities is obtained, it may still differ from measured velocities. This discrepancy can be attributed to the neglect of the radial-flow term if the deviation from axial symmetry as well as the viscous action at the axial station in question are assumed negligible. Figure 3 shows the interpretation of comparison of the measured velocities with velocities computed from simplified radial equilibrium with losses. The shape of the streamline in the r, z surface required to correct a solution for simplified radial equilibrium including an entropy gradient to coincide with measured velocities can be ascertained from such comparisons.

Single Stages

Downstream of guide vanes. - Axial-velocity ratios for the axial station downstream of the guide vanes calculated from measured data and from the solution for simplified radial equilibrium are presented in figures 4 to 8. Axial-velocity ratios calculated from the solution for simplified radial equilibrium including the entropy gradient are presented in figure 4 as an example of the effect of the radial variation of guide-vane losses on the axial-velocity profile downstream of a set of circular-arc sheet-metal guide vanes.

Low hub-tip ratio stages: - The dimensionless axial-velocity profiles presented in figures 4 to 7 were obtained from compressors of low rotor-inlet hub-tip ratio (0.50 to 0.55). These configurations were also similar in flow distribution as well as in geometry: They were designed for wheel-type or wheel-minus-vortex rotor-inlet whirl.

A comparison between the axial-velocity profiles obtained from data and those from the solution for simplified radial equilibrium presented in figures 4 to 7 reveals the same trend for most cases: The solution yields axial velocities which are lower near the tip and higher near the hub than those calculated from data. The only exception to this trend (fig. 4(c)) represents operation at a low-flow coefficient. As discussed in reference 13, rotor operation at low-flow coefficients can result in a recirculating type of flow at the rotor tip. The possible consequences of this type of flow will be brought out in connection with the streamline-curvature and entropy-gradient characteristics.

The axial-velocity profiles obtained from the solution including the entropy gradient are slightly different from those obtained from the simplified-radial-equilibrium solution. The effect of the entropy gradient, for the two cases presented, is to increase slightly the discrepancies at the hub and tip between the axial-velocity ratios obtained from data and those obtained by simplified-radial-equilibrium calculation. (Because this effect was small, and because the available guide-vane-loss data for other configurations indicated approximately the same loss characteristics, the solution including the entropy gradient was not determined for the data of figs. 5 to 7.) For the low-flow case (fig. 4(c)), the recirculating flow at the rotor tip would increase the entropy upstream of the rotor and thereby lower the inlet axial velocity.

The discrepancies between the axial-velocity profiles obtained from data and from the solution for simplified radial equilibrium are probably a consequence both of the assumption of axial symmetry and the neglect of the radial-flow term. The analysis of reference 14 shows that, for guide vanes with a radial circulation gradient, the condition of irrotationality requires that a tangential gradient of radial velocity must exist. The radial component of Euler's equation for steady flow expressed in cylindrical coordinates is as follows:

$$V_r \frac{\partial V_r}{\partial r} + \frac{V_\theta}{r} \frac{\partial V_r}{\partial \theta} + V_z \frac{\partial V_r}{\partial z} - \frac{V_\theta^2}{r} = - \frac{1}{\rho} \frac{\partial p}{\partial r} \quad (15)$$

From equation 15, it can be seen that for such a flow the assumption that $\frac{1}{\rho} \frac{\partial p}{\partial r} = \frac{V_\theta^2}{r}$ is not exact even if $\frac{\partial V_r}{\partial r} = \frac{\partial V_r}{\partial z} = 0$.

3038

If the trend indicated in figures 4 to 7 can be partly attributed to the effect of streamline curvature, this curvature must necessarily be concave with respect to the casing (fig. 3). Because of the type of whirl addition through the guide vanes (wheel or wheel-minus-vortex), the resulting radial pressure gradient tends to force the flow towards the hub as it passes through the guide vanes. As the gas passes from the guide vanes to the rotor, the hub taper causes a curvature of the streamlines ($\partial V_r / \partial z \neq 0$). It is probable, therefore, that at the axial location of the measuring stations this curvature is concave with respect to the casing (fig. 1), except immediately adjacent to the hub; and the trend of figures 4 to 7 is therefore a logical one. For the case of low-flow operation (fig. 4(c)), recirculating flow at the rotor tip would increase the specific mass flow near the rotor hub in proportion to the mean-radius and tip-region mass flow. This effect would decrease the concavity of the streamline and explain the better agreement between calculated and measured axial velocities near the hub.

High hub-tip ratio stages: - The data of figure 8 were obtained from a single-stage compressor with a hub-tip ratio of 0.8 and designed for the addition of wheel-type whirl through the guide vanes. In contrast with the trend of figures 4 to 7, the axial-velocity ratios calculated from the solution for simplified radial equilibrium are slightly lower near the hub and higher near the tip than the data. If the solution for simplified radial equilibrium including the entropy gradient had been obtained (the necessary guide-vane-loss data for such a solution were not available), the calculated axial-velocity ratios probably would have more closely agreed with the data. The indication is that the net effect of the first three terms of equation (15) is negligible. The hub taper is slight for a hub-tip ratio of 0.8 and the guide-vane aspect ratio is low (0.80); therefore, the streamline curvature would be smaller than for the compressor with a hub-tip ratio of 0.5. For this configuration the type of flow distribution has little effect on the importance of the radial-flow term, probably because the small passage depth permits little deviation from a two-dimensional flow.

Downstream of rotor. - Axial-velocity ratios for the axial station downstream of the rotor obtained from data and from the two solutions of simplified radial equilibrium are presented in figures 9 to 17.

Low hub-tip ratio stages: - The data of figures 9 to 13 were obtained from stages having a rotor-inlet hub-tip ratio of 0.55 or less. The design-flow distributions were similar: wheel-type or wheel-minus-vortex rotor-inlet whirl with constant-enthalpy addition through the rotor. The comparisons between axial-velocity profiles obtained from data and from the solution for simplified radial equilibrium indicate a similar trend for each compressor in full-stage configuration, namely, that the calculated values are slightly low near the tip and higher near the hub than the data. However, for the configurations without stators (figs. 12 and 13) good agreement is indicated between measured and calculated axial-velocity profiles. The curves of figure 9 indicate that variation of flow coefficient has little effect on the observed trend that the calculated velocities exceed the data near the hub. The solution for simplified radial equilibrium including the entropy gradient (figs. 9 to 13) is not markedly different from the solution without the entropy gradient.

The trends of figures 9 to 11 are similar to those observed for the data after the guide vanes, and a similar analysis can be applied. As discussed in reference 12, the radial pressure gradient downstream of a rotor with wheel-minus-vortex inlet flow causes a radial flow toward the hub; after the stators the flow shifts toward the casing. The blockage effect of the stators (the fact that they block more of the annular-flow area near the hub than near the casing) also contributes to this shift in flow. Geometrically, the large passage depth and high rotor-blade aspect ratio (2.7 to 3.0) contribute to an appreciable curvature of the streamlines. All these effects tend to make the streamlines concave looking from the casing at the measuring station downstream of the rotor. The velocity comparisons of figures 9 to 11 indicate that the streamlines are concave in these instances. The term of Euler's equation (eq. 15) neglected because of the assumption of axial symmetry might also be significant. The accumulated guide-vane and rotor losses were insufficient to cause, through the entropy gradient, a marked effect on the axial-velocity profiles for the free-stream region.

The trend indicated in figures 12 and 13 of better agreement between calculated and measured axial velocities than is indicated for the same rotors in figures 9 and 10 can probably be explained by the absence of stators. Without stators there is less tendency for a shift in flow downstream of measuring station 2, and the flow probably stabilizes on approximately conical surfaces.

High hub-tip ratio stages: - The configurations from which the data of figures 14 to 17 were obtained have rotor-inlet hub-tip ratios of 0.80 and higher. The most interesting trend is the good agreement between data and the solution for simplified radial equilibrium including the entropy gradient. As was the case for data upstream of the rotor, the indication is that the net effect of streamline curvature and axially

asymmetric flow is negligible. Also, the effect of losses is more appreciable than for the low hub-tip ratio stages, probably because the high hub-tip ratio units operated at higher blade loadings, with consequently higher total-pressure losses, and because the blade-end region constituted a greater proportion of the passage height.

Downstream of stators. - Axial-velocity profiles for low hub-tip ratio stages at the measuring station downstream of the stators are presented in figures 18 to 20. The curves indicate good agreement between data and the calculation including entropy gradient. The entropy gradient was especially significant at low flows (figs. 18(b) and 19(b)). A negligible effect of axially asymmetric flow and radial flow is indicated. The shift in flow towards the casing which occurs through a stator-blade row is augmented by the hub taper. As the flow proceeds downstream from the stators, it tends to stabilize on approximately conical surfaces (if no rotor follows) or is shifted back toward the hub through the following rotor. The analysis of reference 12 indicates that the stream surfaces through a second stage are similar in shape to the hub contour. Thus, the streamline curvature would be small with a negligible effect on the computed axial-velocity profile.

Boundary-layer data. - Supplementary flow measurements were made at radial stations close to the hub and casing and are compared with analytical solutions in figures 21 to 23. Figure 21 shows velocity comparisons after a rotor with a high hub-tip radius ratio where the velocities obtained by using simplified radial equilibrium with an entropy gradient agree with measured velocities. The simplified-radial-equilibrium approximation gives velocities which are high in the casing boundary layer (the region where the axial velocity drops sharply).

A comparison of velocities after a transonic rotor with low hub-tip radius ratio is shown in figure 22. The solution for velocities which does not include an entropy gradient shows again the pattern of velocities which are too high in the tip regions. These analytical velocities, which are too low at most radial stations near the hub, are higher at the radial station nearest the hub than the measured velocities and velocities obtained analytically by using an entropy gradient. The comparison of velocities indicates that the entropy rises sharply in the boundary-layer regions, while in the main-stream region the minimum entropy occurs near the hub and rises gradually toward the tip.

For the available boundary-layer data after stators (fig. 23), the measured velocities and the velocities calculated by using simple radial equilibrium including an entropy gradient agree very closely. Analytical velocities obtained by the simple-radial-equilibrium approximation are markedly high near the hub and tip and low near the mean-radius station; they are more incorrect than the velocities obtained by this type of calculation after the rotor of figure 22.

In general, the close agreement between measured velocities and velocities calculated by using simplified radial equilibrium with an entropy gradient shown in figures 21 to 23 indicates the radial-flow term is unimportant here. For the configuration of figure 21, the high hub-tip radius ratio prevents any large deviations from two-dimensional flow; for the low hub-tip radius ratio stage of figures 21 and 22 there is little tendency for radial flows because of the flow distribution (zero rotor-inlet whirl).

The effect of the entropy gradient outside the boundary layer is greater for the transonic rotor (fig. 22) than for the subsonic inlet-stage compressors (figs. 9 to 11). The transonic rotor has a higher relative inlet Mach number and also a larger radial variation of relative inlet Mach number than the subsonic stages, leading to larger total-pressure losses and larger radial variations in total-pressure losses in the transonic stage. The magnitude of the discrepancy between the two radial-equilibrium solutions is higher after stator than after rotor because of additional losses incurred by the stator-blade row.

The importance of estimating blade-element and boundary-layer losses in design calculations is emphasized by the large discrepancies between the two analytical velocities. The close agreement between data and calculations including an entropy gradient in the boundary-layer regions indicates that the blockage effect of the boundary layer can be taken into account by a design assumption of the boundary-layer stagnation-pressure profile. This assumed profile can be based on available boundary-layer-loss data.

Middle and End Stages of Multistage Compressor

Downstream of rotors. - The configurations in this section differ from those previously discussed in that the entropy gradient is higher since losses have accumulated for several stages. Figure 24 shows data from a rotor which is preceded by four stages of a multistage compressor. Comparisons are made in this case for a range of flow coefficients to ascertain the effect of a wide variety of losses through a specified blade row on the trends of the solutions based on simplified radial equilibrium with an entropy gradient. In all cases, including the entropy gradient in the simplified radial equilibrium, calculations led to good agreement with measured velocities. Similarly, investigations for a large number of flow coefficients were made for the other configurations in this section and showed again that the entropy-gradient correction led to good agreement with measured velocities. Since these comparisons for a variety of flow coefficients are similar to those of figure 24, they are not included in the figures presented.

3038

Velocities after the last rotor of a 10-stage compressor are shown in figure 25. Near design conditions after these rotors (figs. 24(a), 24(b), and 25(a)) the simplified-radial-equilibrium approximation gives velocities which are high for both hub and tip stations and low near the mean radius station, indicating that the shape of the entropy gradient is different from those found in the single-stage comparisons. As pointed out in figure 2(b), the entropy has a minimum value at some intermediate radius between hub and tip, showing that the losses are greatest near the end walls. The growth in losses near the hub for the middle-stage rotors is the most significant change from the loss profiles indicated for the single-stage configurations. These changed profiles may result from the accumulation of losses which occur at the unattached blade ends, on the end walls, or on the blades. Figures 24(c) and (d) show exceptions to this pattern, for here indications are that the entropy increases from hub to tip. These are low-flow-coefficient runs at which the blades might be expected to operate inefficiently, with the tip region being most sensitive to changes in weight flow. As the flow coefficient is decreased (figs. 24(c) and (d)), the losses at the tip regions become highest, changing the entropy gradient pronouncedly.

09-3 back

Downstream of stators. - The inadequacy of simplified-radial-equilibrium approximation after stators is shown clearly in figures 26 and 27. Data after the fifth and ninth stators of a multistage compressor show that the consideration of the entropy term is even more important here than after the rotors. The simplified-radial-equilibrium-approximation solutions give very poor agreement with actual data. After the fifth stator the entropy reaches a pronounced maximum in the end regions of the blade, as indicated by figures 26(a) and (b). Near design conditions after the ninth stator (fig. 27(a)) the same type of entropy gradient as for the fifth stator (fig. 26) is indicated. At off-design conditions (fig. 27(b)) an increase in losses near the casing which occurs after the rotors is also apparent after these stators.

Discussion of multistage results. - The radial-entropy variation in the latter stages of a multistage compressor must be evaluated and used in the equilibrium equation in order to correctly compute axial-velocity profiles. This variation follows a general pattern; at or near design weight flow the entropy has a minimum value near the mean radius, increasing toward each of the end walls, while at flow coefficients other than design the entropy has a minimum at the hub region and increases monotonically toward the tip.

ANALYSIS OF DESIGN TECHNIQUE

Application of Radial-Equilibrium Equation

In view of the results of the experimental investigation, it would be desirable to use a procedure based on equation (9) in the calculation

of velocity diagrams for the design of a multistage machine. In an axial-flow turbomachine design, the variables which will be known or assumed are the inlet conditions to the blade row, the desired weight flow, and the losses or adiabatic efficiency of each blade element. The radial gradient of energy addition is usually prescribed through an analytical variation of either V_θ or ΔH with radius. In order to obtain the total-pressure rise from the total-temperature rise, the blade-element total-pressure losses must be known or assumed as functions of the velocity-diagram parameters. For instance, the relative total-pressure-loss parameter $\bar{\omega}$ is presented in reference 14, wherein the relative-total-pressure loss is given as a function of relative inlet Mach number and a blade-loading parameter, the diffusion factor D . A preliminary solution of the simplified-radial-equilibrium approximation can be obtained in order to calculate D factors, or the diffusion factors can be assumed on the basis of previous experience. This assumed radial variation in losses now yields an assumed radial variation in entropy, since from equation (5a)

$$\frac{s_2}{R} = \frac{s_0}{R} + \ln \left[\left(\frac{T_2}{T_0} \right)^{\frac{\gamma}{\gamma-1}} \frac{P_2}{P_0} \right] \quad (5b)$$

A first approximation to the axial-velocity profile after the rotor can now be found by using equation (9). By selecting a value for $V_{z,2}$ at the mean radius, using this as $V_{z,2,k'}$ and solving for $V_{z,2,u}$ at the next stations toward hub and tip, the velocities across the entire passage can be found by repeating the process with the results of each step used as reference values in the next step. Since the method gives accurate profiles (if blade-element and end-wall-loss data are available) across the passage from hub to casing, corrections such as blockage factor or boundary-layer displacement thickness are unnecessary for the continuity equation.

Solution for Velocity Distributions

The design procedure will vary depending on whether the passage area or mean-axial-velocity variation is fixed through the machine. In both cases an iteration process will be necessary and the attacks will be similar. An example will be made for a rotor with a fixed passage area (r_h and r_t known). This is the type of calculation which might be applied after a preliminary analysis on a mean-radius basis has determined the hub contour (for a fixed-tip-radius machine). In this case the following factors would be known or assumed:

3038

- (1) Hub and tip radii throughout the machine
- (2) Weight flow
- (3) Rotative speed
- (4) Inlet total temperature and pressure

A convenient design method is to prescribe the outlet radial variation of tangential velocity (hence the energy addition in the case of a rotor). For simplicity, the streamline flow is assumed to occur at equal increments along the radius, thus fixing r_2 as a function of r_1 . The total-temperature rise across the rotor can now be found at each radial position from the equation

$$c_p(T_2 - T_1) = (U_2 V_{\theta,2} - U_1 V_{\theta,1}) \quad (16)$$

In addition to the requirement that equation (9) be satisfied after the blade row, the continuity equation (13) must also be satisfied at this axial station. Since the variation of static temperature with radius is generally small $\left(\frac{t_t - t_h}{t_m} = 0\right)$, a first approximation may be made by assuming that $t = \text{constant}$ and is equal to the value at r_k . Equation (9) combined with equation (10) then yields the following equation:

$$V_{z,2,u}^2 = 2R \left(T - \frac{V_{2,k}^2}{2c_p} \right) \left\{ \ln \left[\frac{\left(\frac{T_{2,k}}{T_0} \right)^{\frac{\gamma}{\gamma-1}}}{\frac{P_{2,k}}{P_0}} \right] - \ln \left[\frac{\left(\frac{T_{2,u}}{T_0} \right)^{\frac{\gamma}{\gamma-1}}}{\frac{P_{2,u}}{P_0}} \right] \right\} +$$

$$V_{\theta,2,k}^2 - V_{\theta,2,u}^2 + V_{z,2,k}^2 + 2 \int_{r_u}^{r_k} \frac{V_{\theta,2}^2}{r_2} dr_2 + 2c_p(T_{2,u} - T_{2,k}) \quad (17)$$

This solution must be corrected to obtain the proper weight flow. With the use of the values of $V_{z,2}$ obtained from solutions of equation (17), the equation for continuity can be solved (by using eqs. (13) and (14)) and an integrated weight flow at station 2 obtained. If the integrated weight flow is within 2 percent of the desired flow, a simple adjustment of all the velocities by the ratio of flows will suffice. Otherwise, the original assumption of mean axial velocity must be adjusted by the ratio of flows and equation (17) again solved.

If the axial-velocity distribution (which is combined with prescribed tangential velocity distribution to give flow angles) which results from these solutions is much different from the expected distribution (causing the D factors to be different from those expected), an adjustment of the assumed blade-element losses may be in order, and a new solution obtained on this basis. This adjustment could also be made as a refinement of the method after a tentative choice of blade shapes is made and the best available blade-element total-pressure-loss data are applied.

In any solution for the precise velocity distribution after a blade row, the need for blade-element- and end-region-loss information is evident. This is especially true in multistage-compressor calculations where blade-element-loss accumulations may cause an appreciable radial gradient of entropy in the latter stages with resulting large effects on the axial-velocity distributions.

SUMMARY OF RESULTS

The investigation of the validity of application of the simplified-radial-equilibrium equation to compressors gave the following results:

1. In order to calculate accurately the radial variation of velocities, it was necessary, in general, to include measured stagnation-pressure losses in the simplified-radial-equilibrium equation. The assumption of zero radial entropy gradient was invalid for the calculation of velocities at axial stations more than one or two blade rows downstream from a region of uniform entropy. At an axial station following several stages of a multistage compressor, large discrepancies were observed between measured velocities and velocities computed by using the simplified-radial-equilibrium equation but neglecting the entropy gradient; whereas the velocities computed by using the entropy gradient agreed closely with the data.

2. Very close agreement was observed between data and the calculations made by using an entropy gradient in the boundary-layer regions at the hub and tip; whereas the calculations which did not include the entropy gradient were not correct. This trend suggests that the blockage effect of the boundary layer can be taken into account by a design assumption of the boundary-layer stagnation-pressure profile based upon available boundary-layer-loss data.

3038

3. Results of this investigation suggest that a velocity-diagram design method including the effect of the estimated stagnation-pressure losses on the design axial-velocity profile would give more accurate velocity diagrams than present methods which do not include stagnation-pressure losses. A velocity-diagram design method including stagnation-pressure losses is presented in this report.

Lewis Flight Propulsion Laboratory
National Advisory Committee for Aeronautics
Cleveland, Ohio, January 27, 1954

3038

REFERENCES

1. Wu, Chung-Hua, and Wolfenstein, Lincoln: Application of Radial-Equilibrium Condition to Axial-Flow Compressor and Turbine Design. NACA Rep. 955, 1950. (Supersedes NACA TN 1795.)
2. Marble, Frank E., and Michelson, Irving: Analytical Investigation of Some Three Dimensional Flow Problems in Turbo-Machines. NACA TN 2614, 1952.
3. Traupel, Walter (C. W. Smith, trans.): New General Theory of Multi-stage Axial Flow Turbomachines. Navships 250-455-1, Navy Dept., Washington (D. C.).
4. Robbins, William H., and Glaser, Frederick W.: Investigation of an Axial-Flow-Compressor Rotor with Circular-Arc Blades Operating up to a Rotor-Inlet Relative Mach Number of 1.22. NACA RM E53D24, 1953.
5. Jackson, Robert J.: Effects on the Weight-Flow Range and Efficiency of a Typical Axial-Flow Compressor Inlet Stage that Result from the Use of a Decreased Blade Camber or Decreased Guide-Vane Turning. NACA RM E52G02, 1952.
6. Budinger, Ray E., and Serovy, George K.: Investigation of a 10-Stage Subsonic Axial-Flow Research Compressor. IV - Individual Stage Performance Characteristics. NACA RM E53C11, 1953.
7. Standahar, Raymond M., and Serovy, George K.: Some Effects of Changing Solidity by Varying the Number of Blades on Performance of an Axial-Flow Compressor Stage. NACA RM E52A31, 1952.
8. Moses, J. J., and Serovy, G. K.: Some Effects of Blade Trailing-Edge Thickness on Performance of a Single-Stage Axial-Flow Compressor. NACA RM E51E28, 1951.
9. Mahoney, John J., Dugan, Paul D., Budinger, Ray E., and Goelzer, H. Fred: Investigation of Blade-Row Flow Distribution in Axial-Flow-Compressor Stage Consisting of Guide Vanes and Rotor-Blade Row. NACA RM E50G12, 1950.
10. Schwenk, Francis C., Lieblein, Seymour, and Lewis, George W., Jr.: Experimental Investigation of an Axial-Flow Compressor Inlet Stage Operating at Transonic Relative Inlet Mach Numbers. III - Blade-Row Performance of Stage with Transonic Rotor and Subsonic Stator at Corrected Tip Speeds of 800 and 1000 Feet Per Second. NACA RM E53G17, 1953.

11. Lieblein, Seymour, Schwenk, Francis C., and Broderick, Robert L.: Diffusion Factor for Estimating Losses and Limiting Blade Loadings in Axial-Flow-Compressor Blade Elements. NACA RM E53D01, 1953.
12. Wu, Chung-Hua: Subsonic Flow of Air Through a Single-Stage and a Seven-Stage Compressor. NACA TN 2961, 1953.
13. Finger, Harold B., and Dugan, James F., Jr.: Analysis of Stage Matching and Off-Design Performance of Multistage Axial-Flow Compressors. NACA RM E52D07, 1952.
14. Lieblein, Seymour, and Ackley, Richard H.: Secondary Flows in Annular Cascades and Effects on Flow in Inlet Guide Vanes. NACA RM E51G27, 1951.

3038

CQ-4

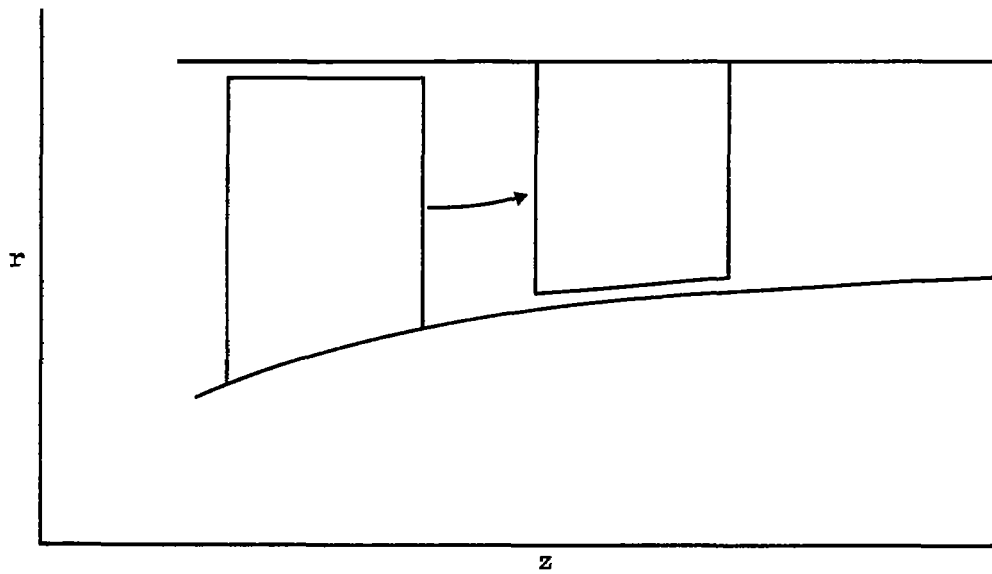
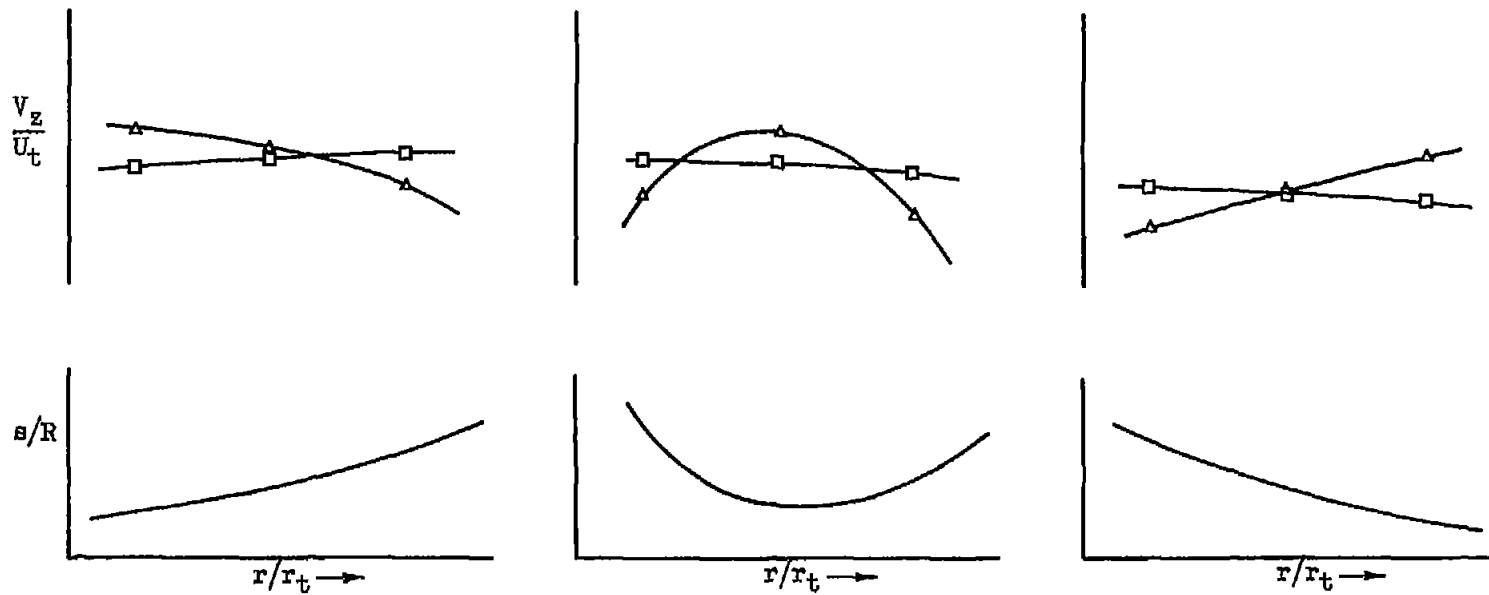


Figure 1. - Streamline in r, z plane, concave looking from compressor casing.

□ Simplified radial equilibrium
 △ Simplified radial equilibrium with entropy gradient

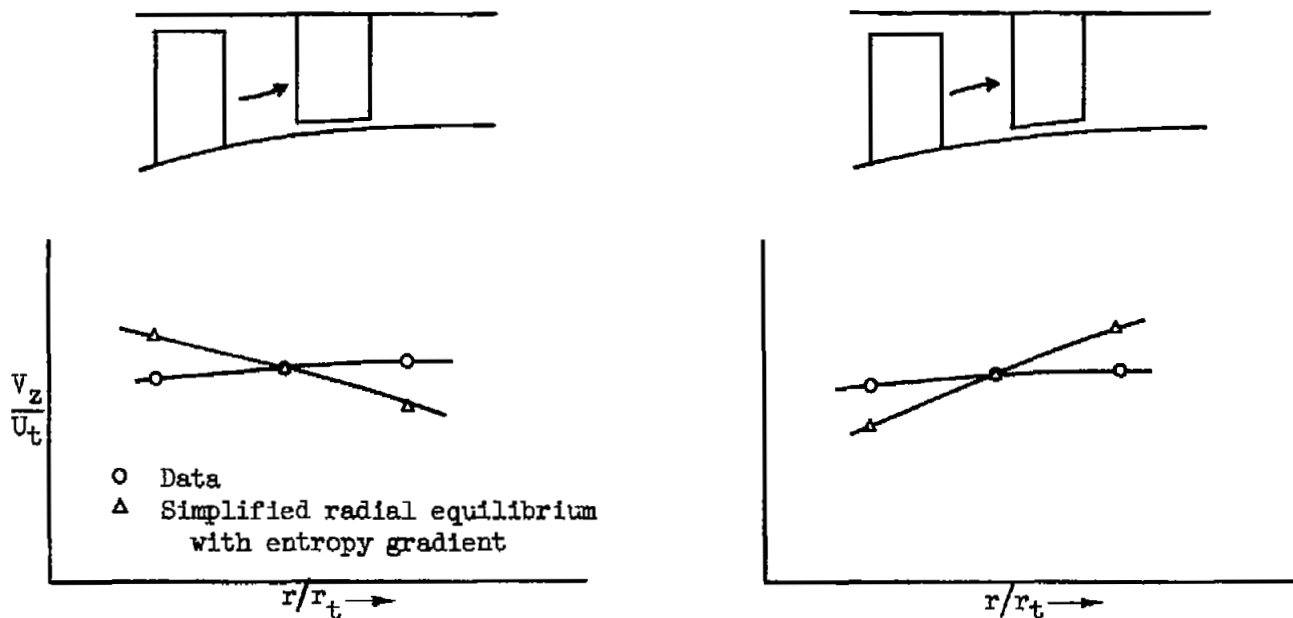


(a) Minimum entropy at hub.

(b) Minimum entropy at mean.

(c) Minimum entropy at tip.

Figure 2. - Effect of entropy-gradient term on simplified-radial-equilibrium solutions.

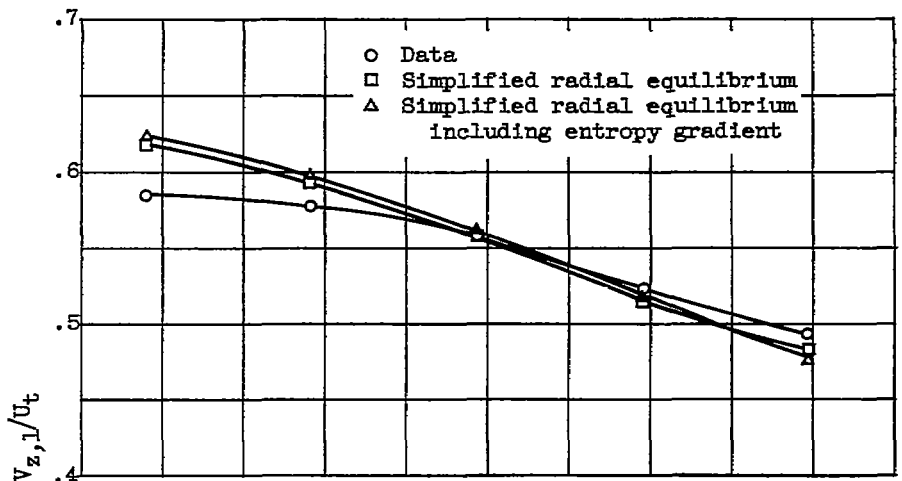


(a) Streamlines indicated to be concave looking from casing.

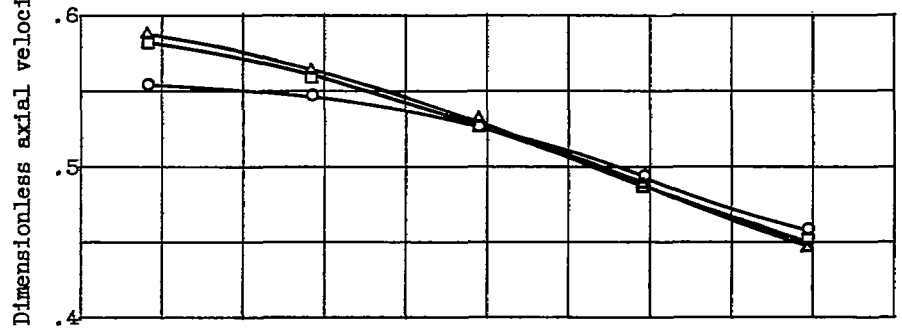
(b) Streamlines indicated to be convex looking from casing.

Figure 3. - Interpretation of comparison of measured velocities with solutions obtained by using simplified radial equilibrium including entropy gradient.

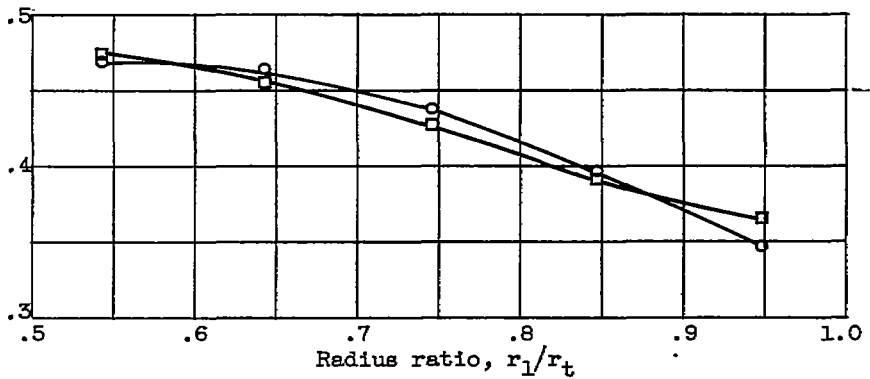
3038



(a) High flow ϕ_1 , 0.525.



(b) Peak efficiency point ϕ_1 , 0.493.



(c) Low flow ϕ_1 , 0.375.

Figure 4. - Simplified-radial-equilibrium axial-velocity comparison after guide vanes for single-stage compressor. Rotor-plus-guide-vane investigation for configuration of reference 4: wheel-type inlet whirl; rotor-inlet hub-tip ratio, 0.5; guide-vane aspect ratio, 2.7; 100 percent design speed.

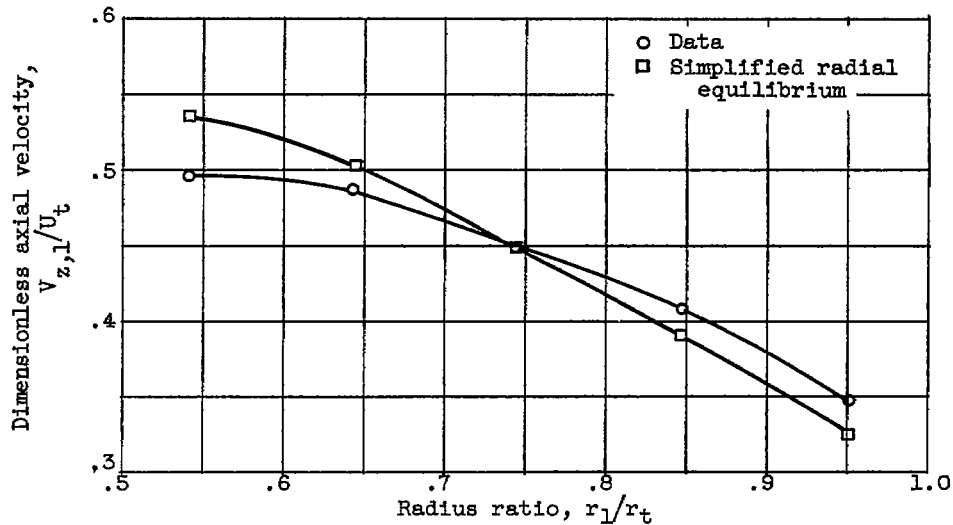


Figure 5. - Simplified-radial-equilibrium axial-velocity comparison after guide vanes for single-stage compressor. Rotor-plus-guide-vane investigation for configuration of reference 5 (low-cambered design): wheel-minus-vortex inlet whirl; rotor-inlet hub-tip ratio, 0.5; guide-vane aspect ratio, 2.9; 100 percent design speed.

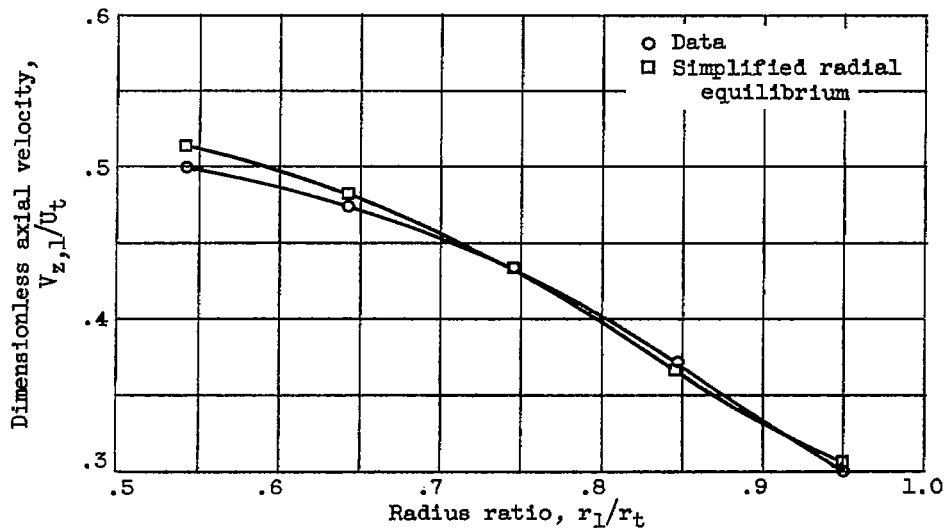


Figure 6. - Simplified-radial-equilibrium axial-velocity comparison after guide vanes for single-stage compressor. Rotor-plus-guide-vane investigation for configuration of reference 5 (high-cambered design): wheel-minus-vortex inlet whirl; rotor-inlet hub-tip ratio, 0.5; guide-vane aspect ratio, 2.9; 100 percent design speed.

3038

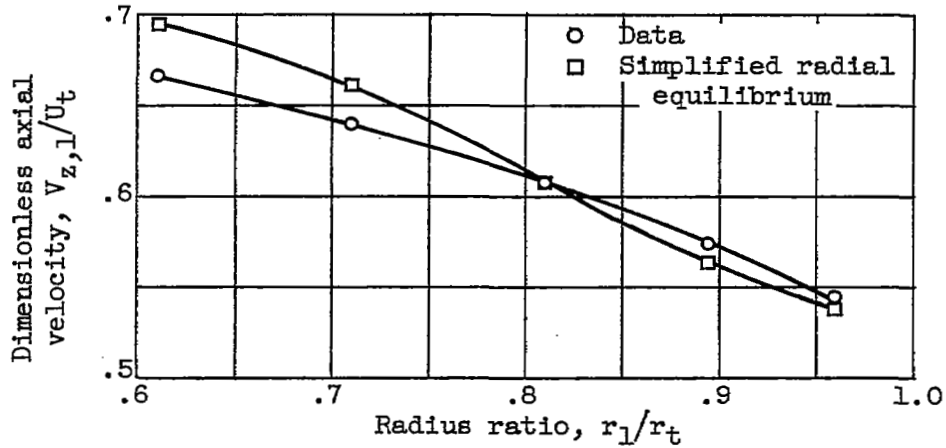


Figure 7. - Simplified-radial-equilibrium axial-velocity comparison after guide vanes for 10-stage compressor. Multistage-compressor investigation for configuration of reference 6: wheel-minus-vortex inlet whirl; rotor-inlet hub-tip ratio, 0.55; guide-vane aspect ratio, 2.6; 90 percent design speed.

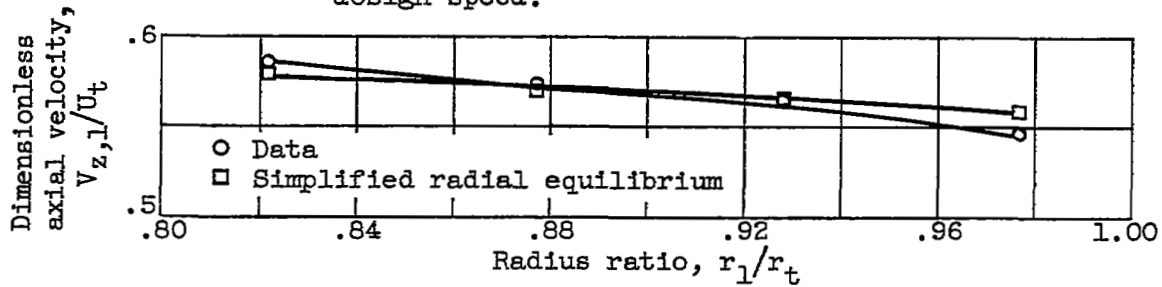
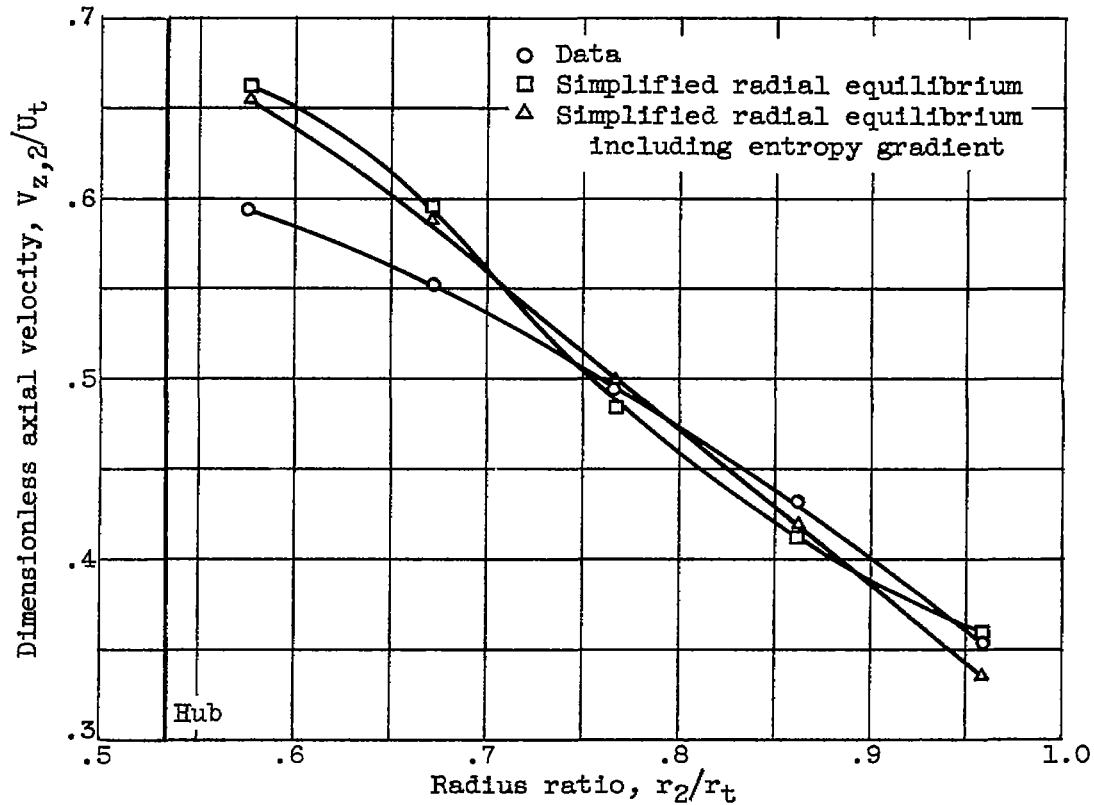
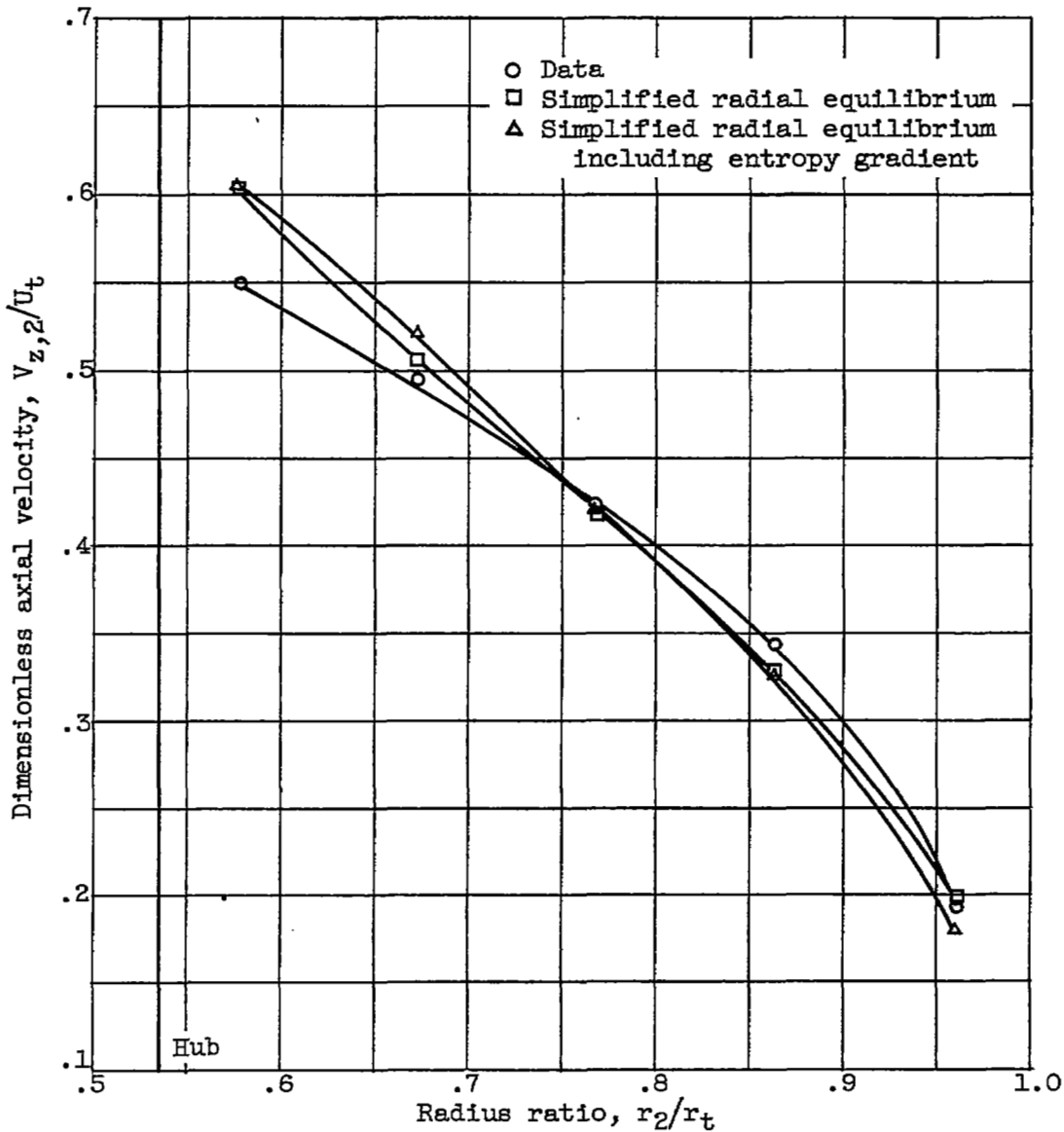


Figure 8. - Simplified-radial-equilibrium axial-velocity comparison after guide vanes for single-stage compressor. Full-stage investigation for configuration of reference 7: wheel-type inlet whirl; rotor-inlet hub-tip ratio, 0.8; guide-vane aspect ratio, 0.8; 100 percent design speed.



(a) High flow φ_1 , 0.445.

Figure 9. - Simplified-radial-equilibrium axial-velocity comparison after rotor for single-stage compressor. Full-stage investigation for configuration of reference 5 (high-cambered design) plus 65-series stator blades: wheel-minus-vortex inlet whirl; rotor-inlet hub-tip ratio, 0.5; rotor-blade aspect ratio, 2.7; 100 percent design speed.



(b) Peak efficiency point ϕ_1 , 0.386.

Figure 9. - Continued. Simplified-radial-equilibrium axial-velocity comparison after rotor for single-stage compressor. Full-stage investigation for configuration of reference 5 (high-cambered design) plus 65-series stator blades: wheel-minus-vortex inlet whirl; rotor-inlet hub-tip ratio, 0.5; rotor-blade aspect ratio, 2.7; 100 percent design speed.

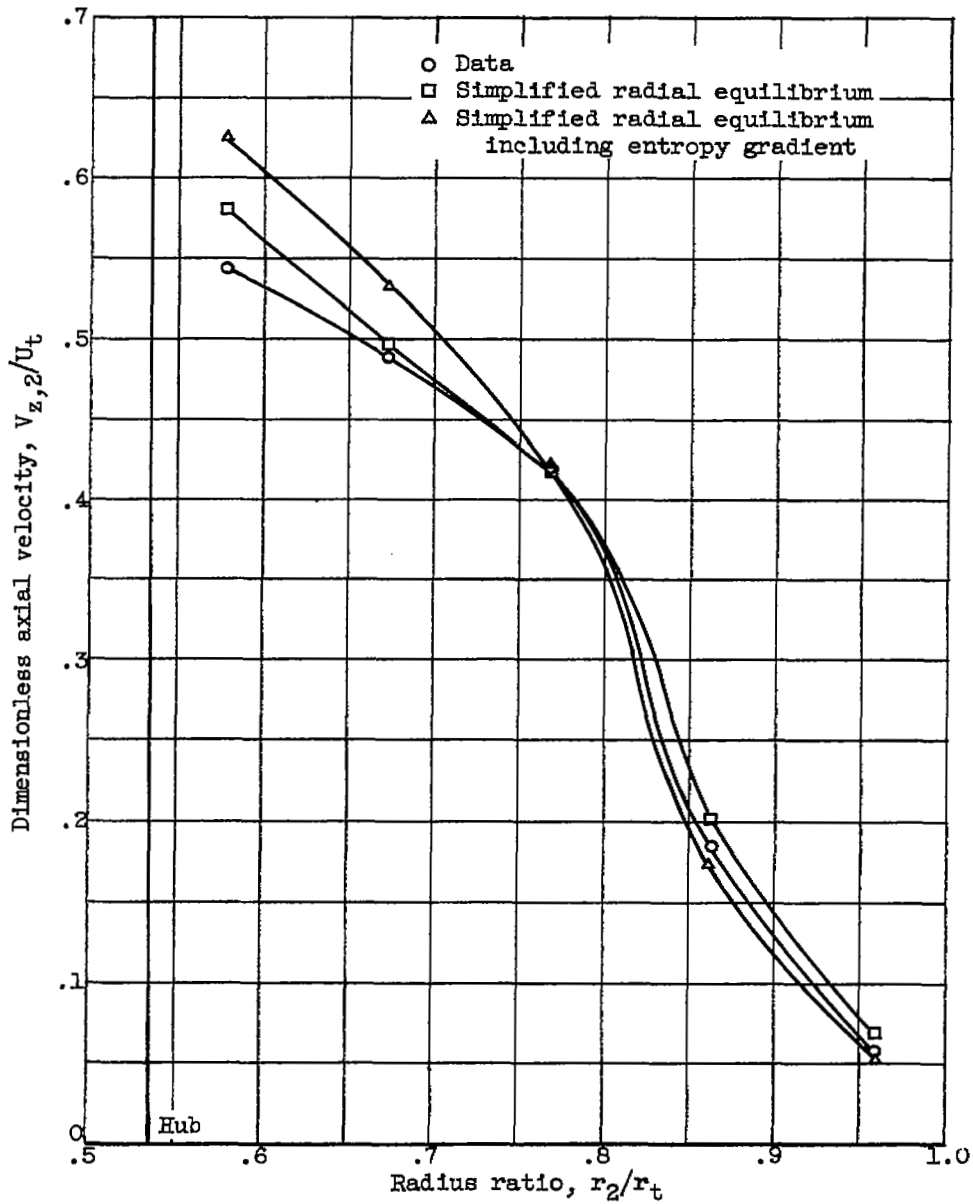
(c) Low flow ϕ_1 , 0.288.

Figure 9. - Concluded. Simplified-radial-equilibrium axial-velocity comparison after rotor for single-stage compressor. Full-stage investigation for configuration of reference 5 (high-cambered design) plus 65-series stator blades: wheel-minus-vortex inlet whirl; rotor-inlet hub-tip ratio, 0.5; rotor-blade aspect ratio, 2.7; 100 percent design speed.

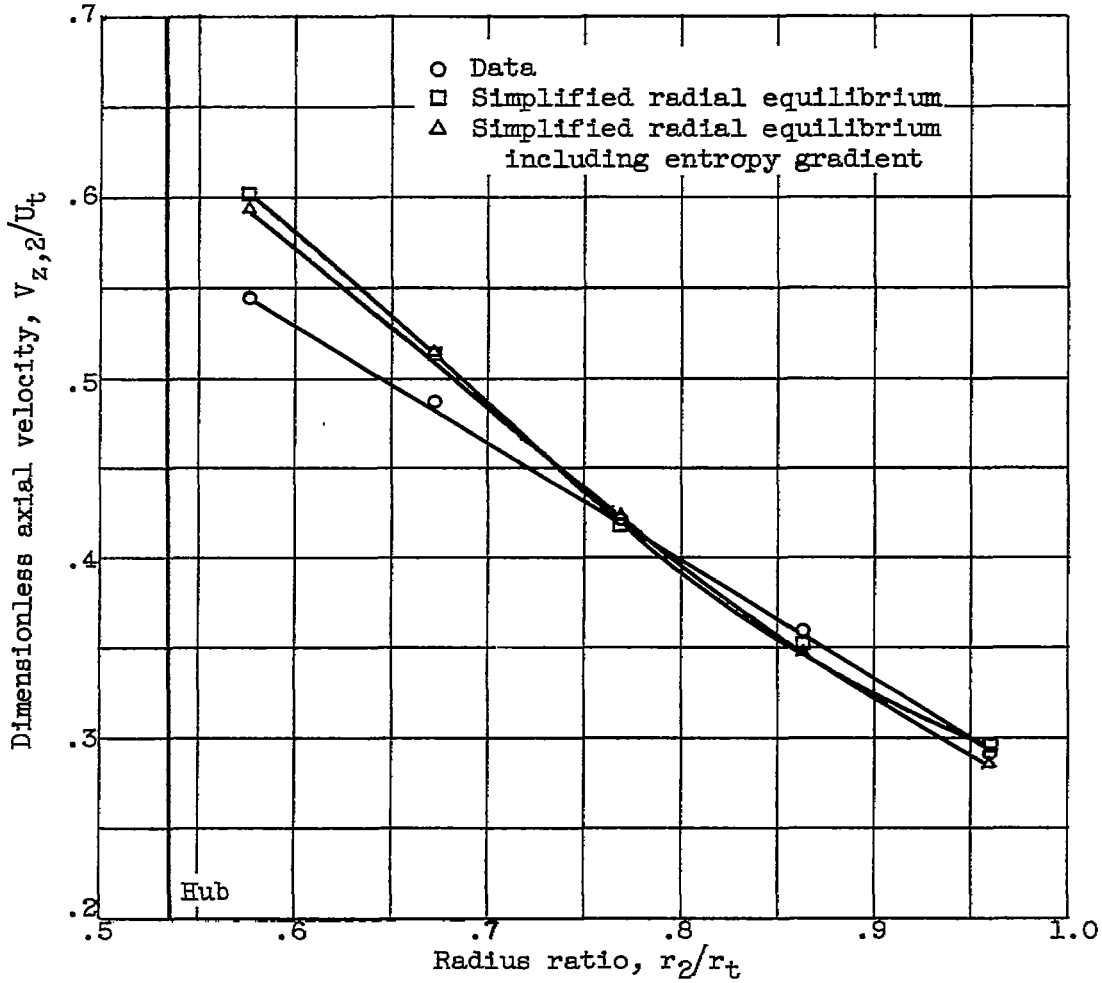


Figure 10. - Simplified-radial-equilibrium axial-velocity comparison after rotor for single-stage compressor. Full-stage investigation for configuration of reference 5 (low-cambered design) plus 65-series stator blades: wheel-minus-vortex inlet whirl; rotor-inlet hub-tip ratio, 0.5; rotor-blade aspect ratio, 2.7; 100 percent design speed.

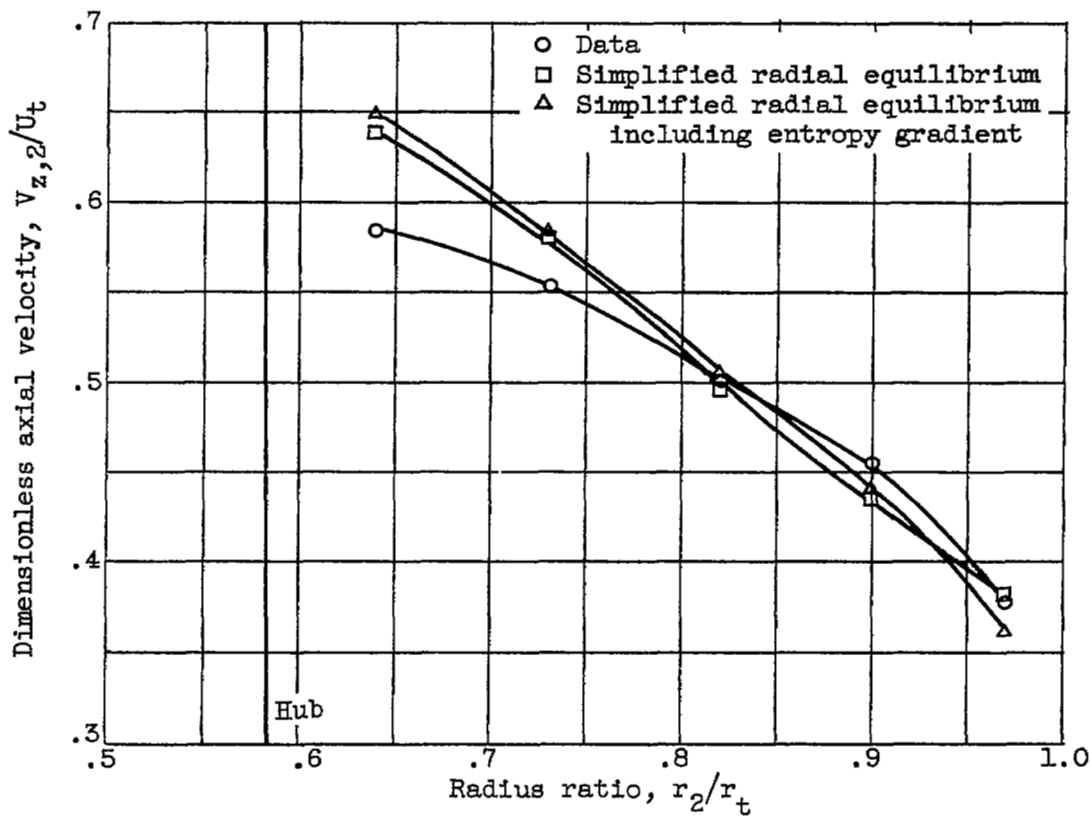


Figure 11. - Simplified-radial-equilibrium axial-velocity comparison after first rotor for 10-stage compressor. Multistage-compressor investigation for configuration of reference 6: wheel-minus-vortex inlet whirl; rotor-inlet hub-tip ratio, 0.55; rotor-blade aspect ratio, 3.0; 90 percent design speed.

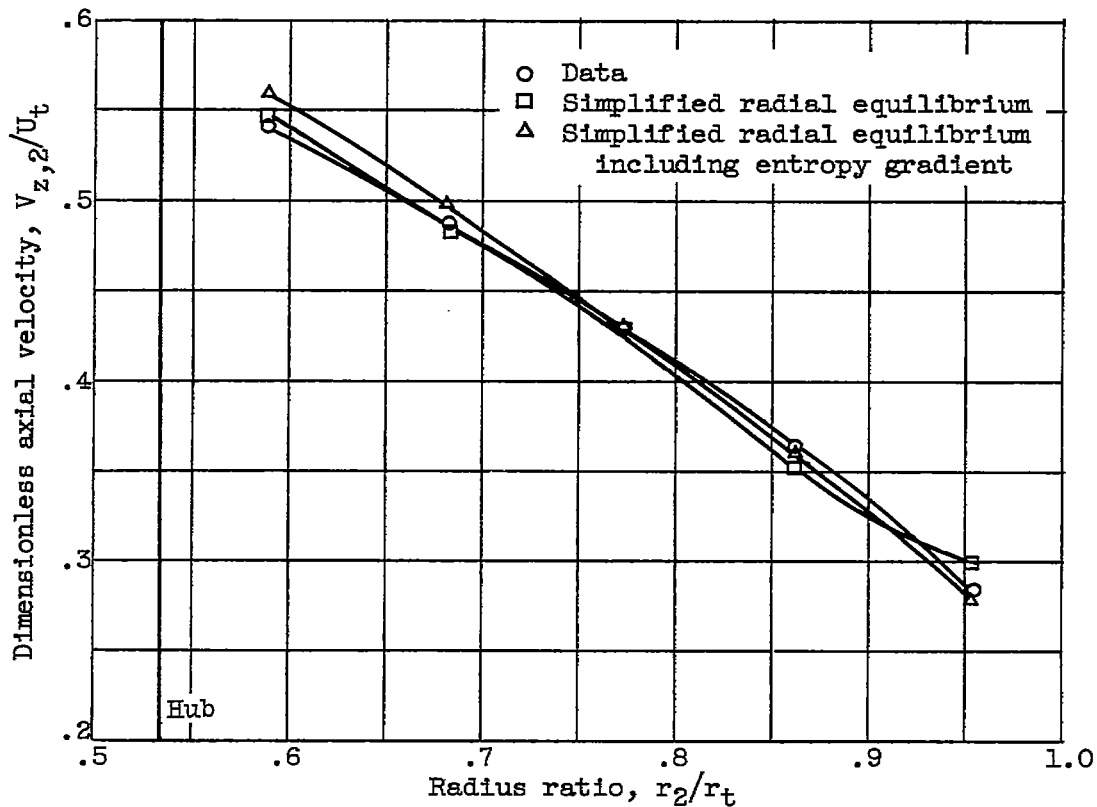


Figure 12. - Simplified-radial-equilibrium axial-velocity comparison after rotor for single-stage compressor. Rotor-plus-guide-vane investigation for configuration of reference 5 (low-cambered design): wheel-minus-vortex inlet whirl; rotor-inlet hub-tip ratio, 0.5; rotor-blade aspect ratio, 2.7; 100 percent design speed.

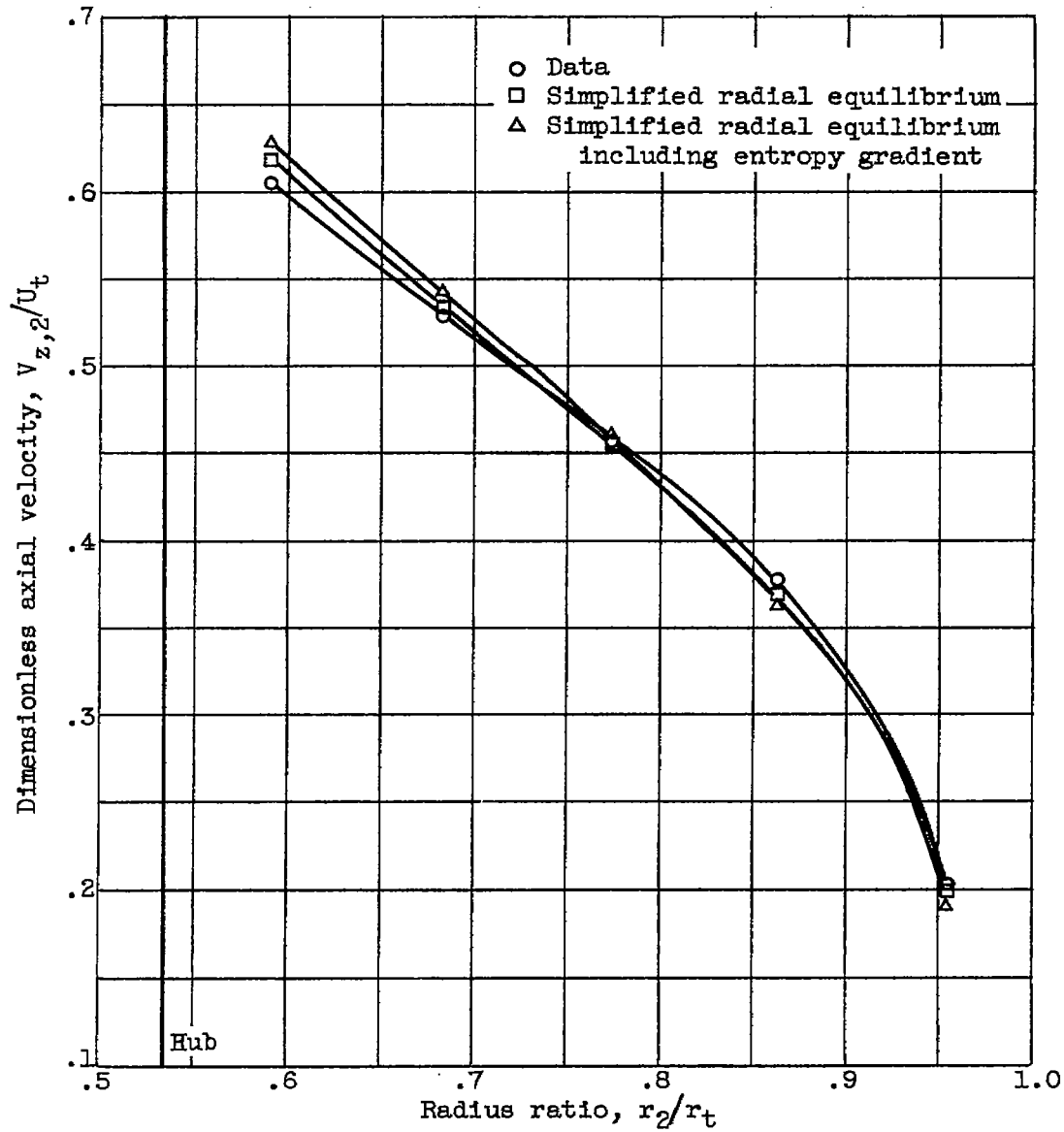


Figure 13. - Simplified-radial-equilibrium axial-velocity comparison after rotor for single-stage compressor. Rotor-plus-guide-vane investigation for configuration of reference 5 (high-cambered design): wheel-minus-vortex inlet whirl; rotor-inlet hub-tip ratio, 0.5; rotor-blade aspect ratio, 2.7; 100 percent design speed.

3038

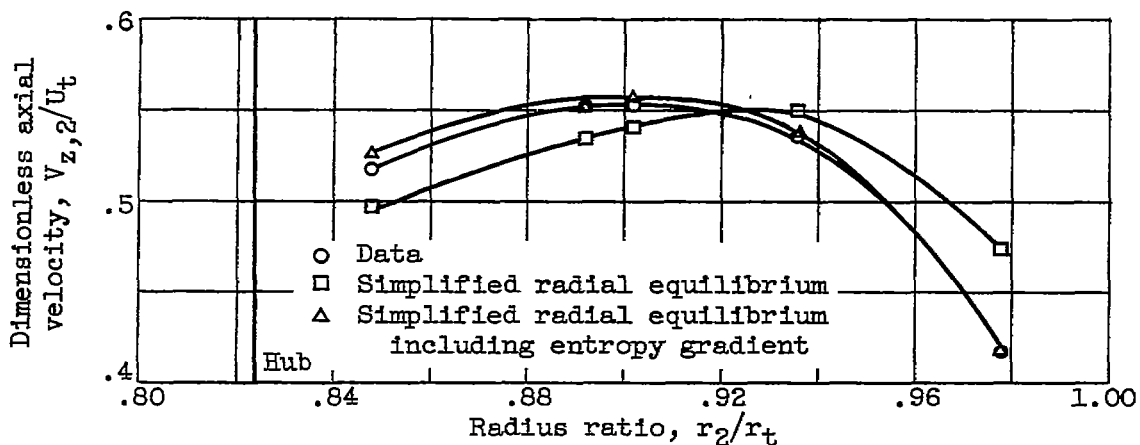


Figure 14. - Simplified-radial-equilibrium axial-velocity comparison after rotor for single-stage compressor. Rotor investigation for configuration of reference 8: zero inlet whirl; rotor-inlet hub-tip ratio, 0.8; rotor-blade aspect ratio, 0.74; 124 percent design speed.

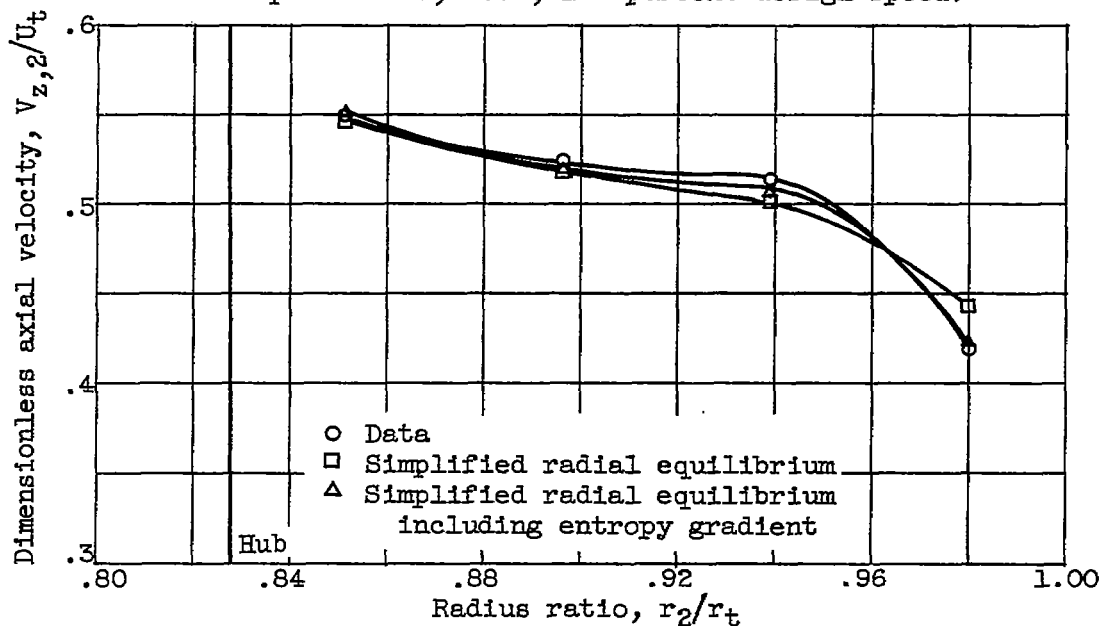


Figure 15. - Simplified-radial-equilibrium axial-velocity comparison after rotor for single-stage compressor. Full-stage investigation for configuration of reference 7 (high solidity): wheel-type inlet whirl; rotor-inlet hub-tip ratio, 0.8; rotor-blade aspect ratio, 0.88; 100 percent design speed.

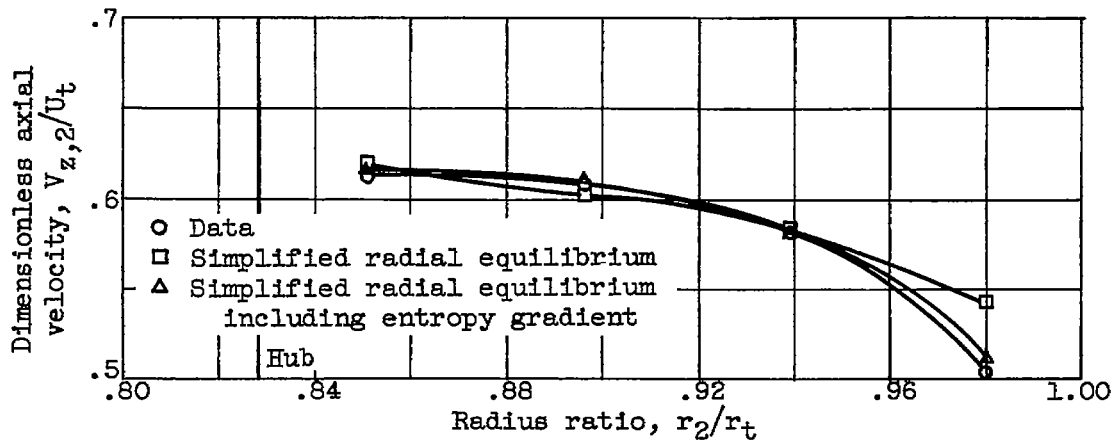


Figure 16. - Simplified-radial-equilibrium axial-velocity comparison after rotor for single-stage compressor. Full-stage investigation for configuration of reference 7 (medium solidity): wheel-type inlet whirl; rotor-inlet hub-tip ratio, 0.8; rotor-blade aspect ratio, 0.88; 100 percent design speed.

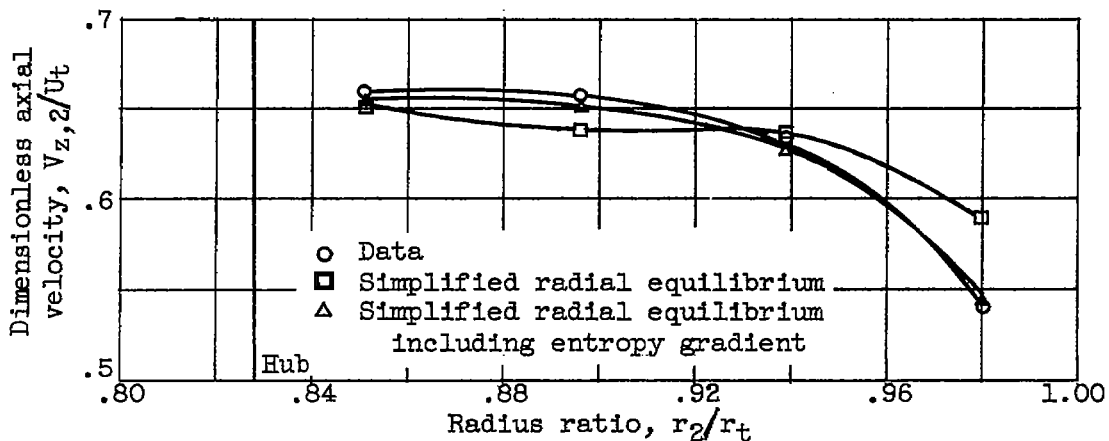
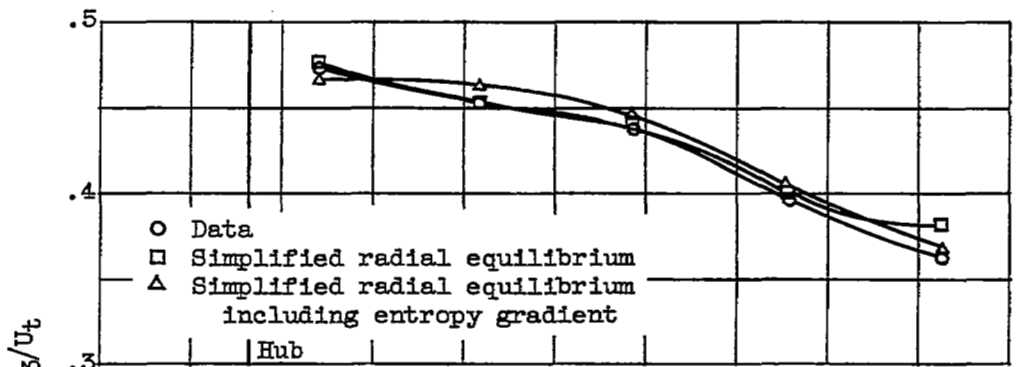
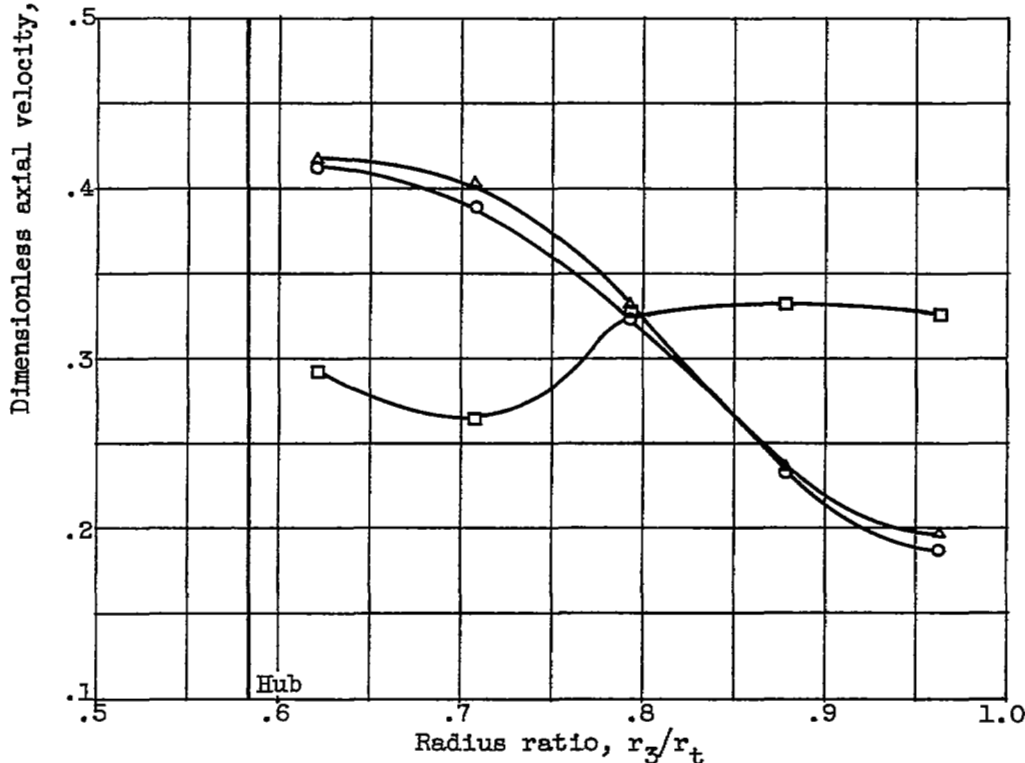


Figure 17. - Simplified-radial-equilibrium axial-velocity comparison after rotor for single-stage compressor. Full-stage investigation for configuration of reference 7 (low solidity): wheel-type inlet whirl; rotor-inlet hub-tip ratio, 0.8; rotor-blade aspect ratio, 0.88; 100 percent design speed.



(a) Peak efficiency point $\phi_1, 0.386$.



(b) Low flow $\phi_1, 0.253$.

Figure 18. - Simplified-radial-equilibrium axial-velocity comparison after stator for single-stage compressor. Full-stage investigation for configuration of reference 5 (low-cambered design) plus 65-series stator blades: wheel-minus-vortex rotor-inlet whirl; rotor-inlet hub-tip ratio, 0.5; stator-blade aspect ratio, 2.5; 100 percent design speed.

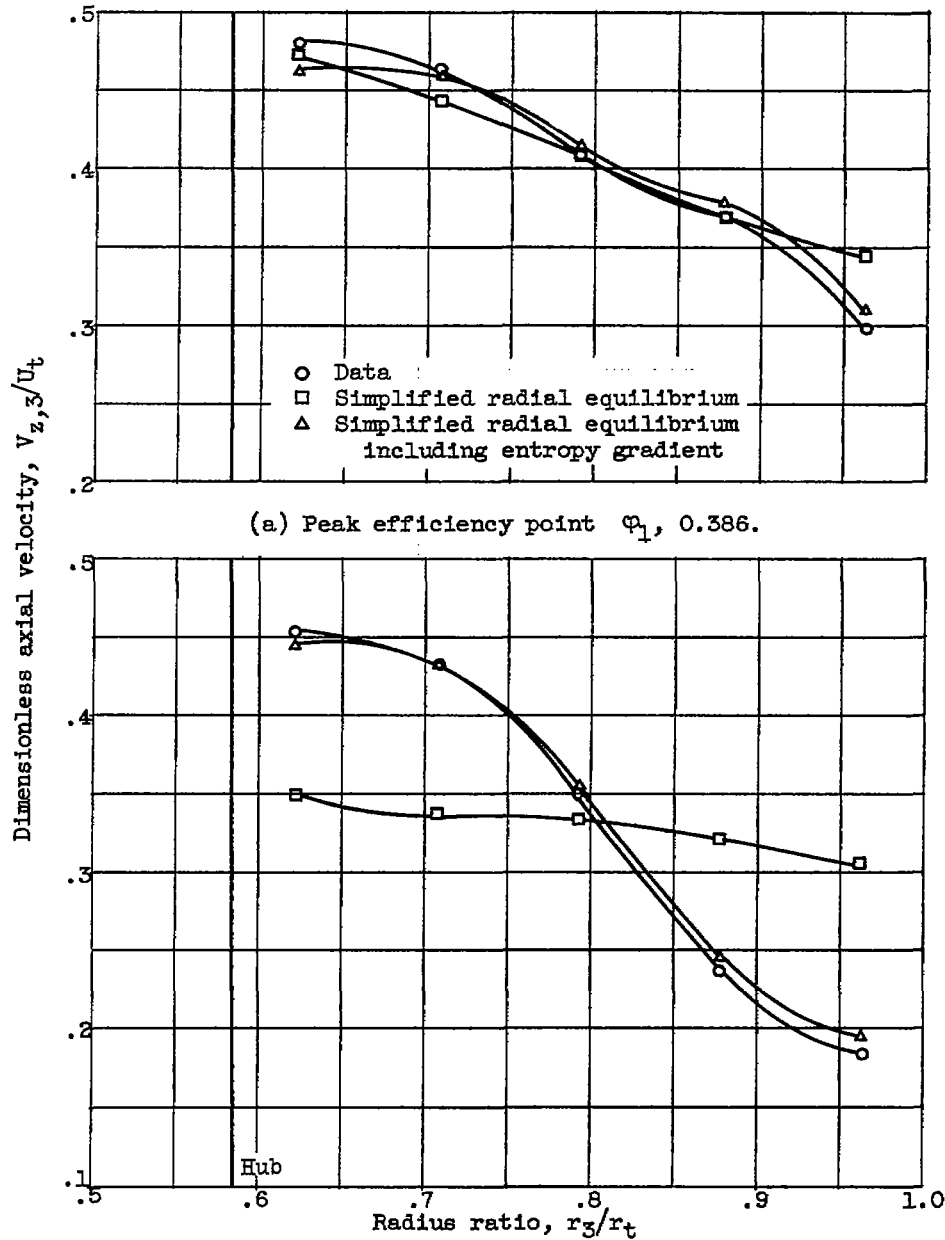


Figure 19. - Simplified-radial-equilibrium axial-velocity comparison after stator for single-stage compressor. Full-stage investigation for configuration of reference 5: wheel-minus-vortex inlet whirl; rotor-inlet hub-tip ratio, 0.5; stator-blade aspect ratio, 2.5; 100 percent design speed.

3038

CQ-6 back

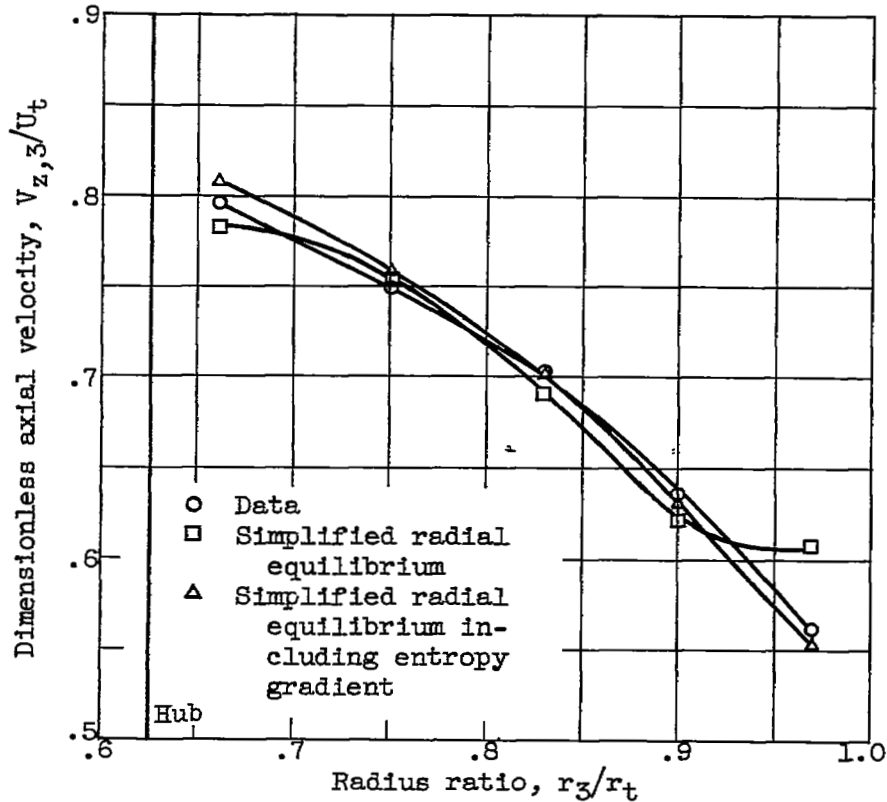


Figure 20. - Simplified-radial-equilibrium axial-velocity comparison after first stator of 10-stage compressor. Multistage-compressor investigation for configuration of reference 6: wheel-minus-vortex inlet whirl; rotor-inlet hub-tip ratio, 0.55; stator-blade aspect ratio, 2.8; 100 percent design speed.

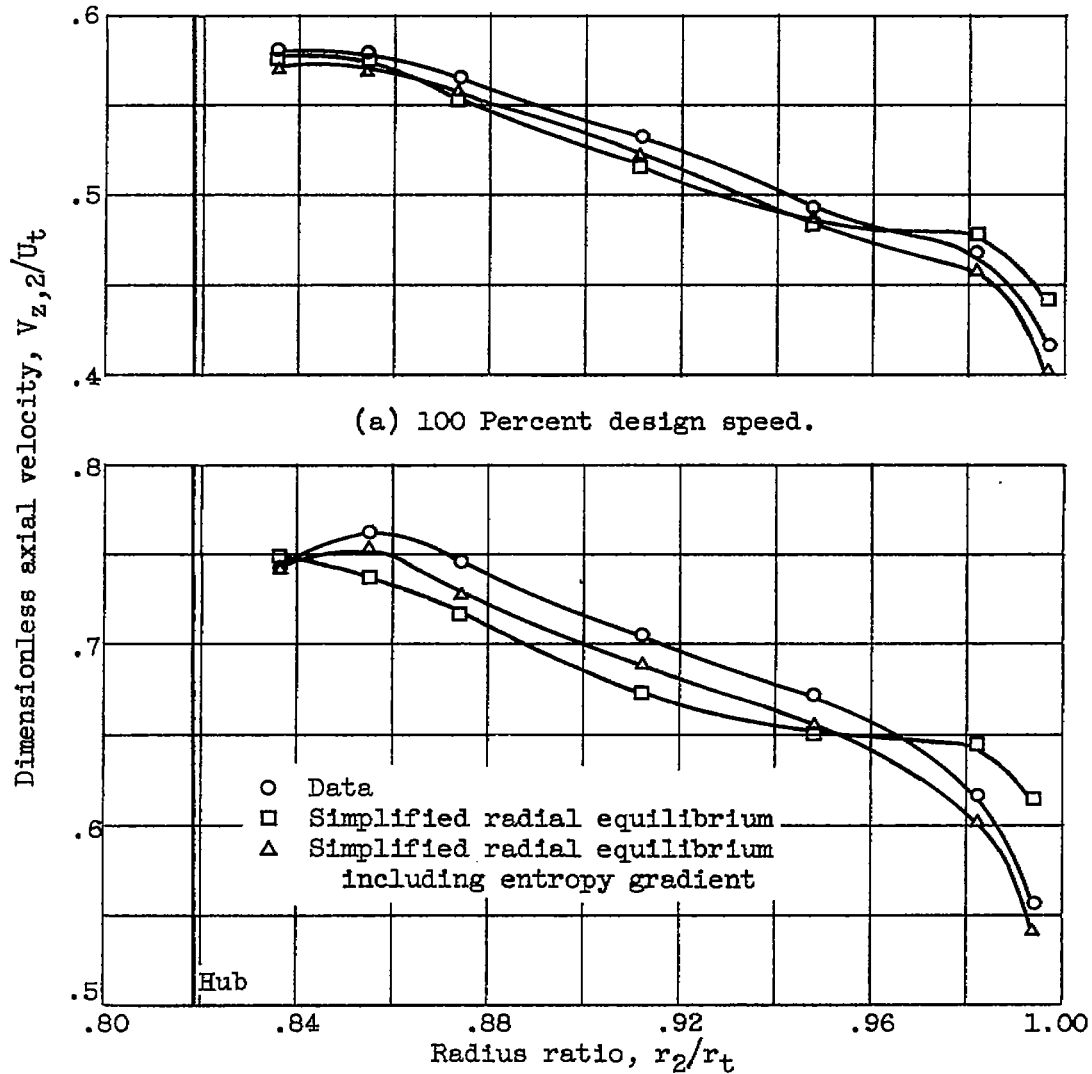


Figure 21. - Simplified-radial-equilibrium axial-velocity comparison after rotor for single-stage compressor. Boundary-layer investigation for configuration of reference 9 for rotor plus guide vanes: wheel-type inlet whirl; rotor-inlet hub-tip ratio, 0.8; rotor-blade aspect ratio, 1.1.

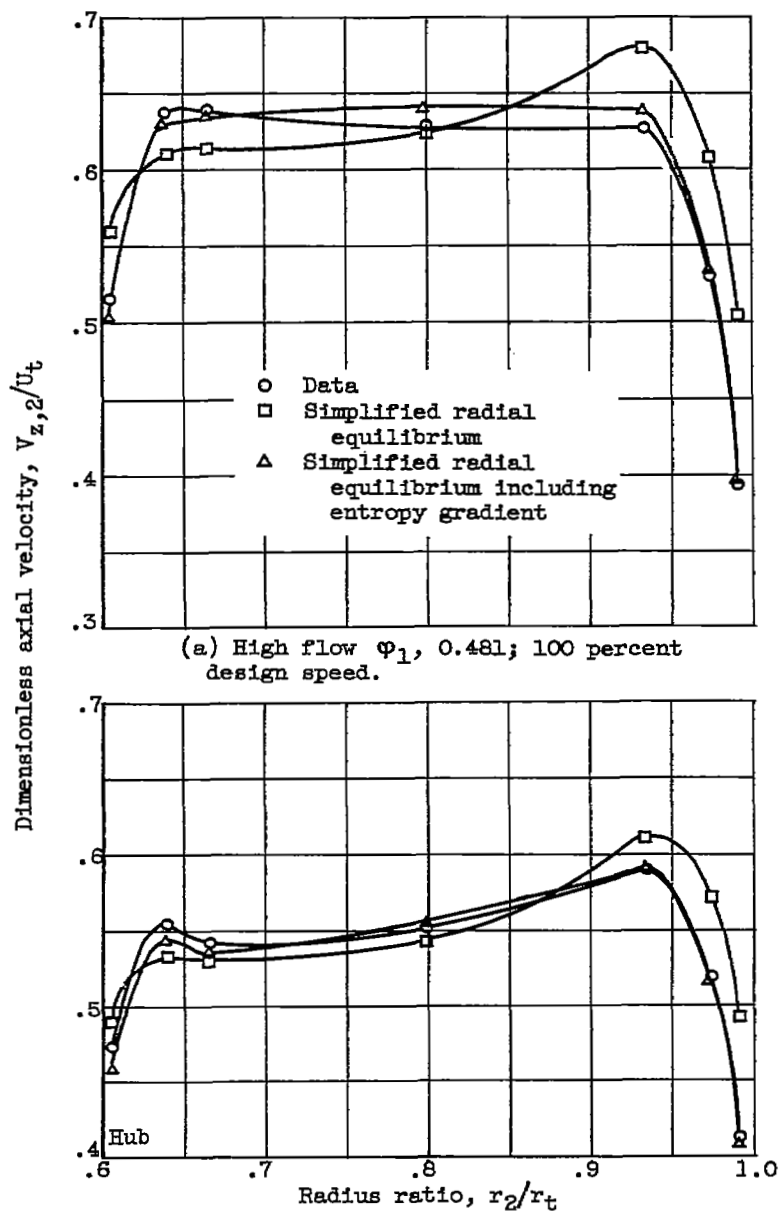
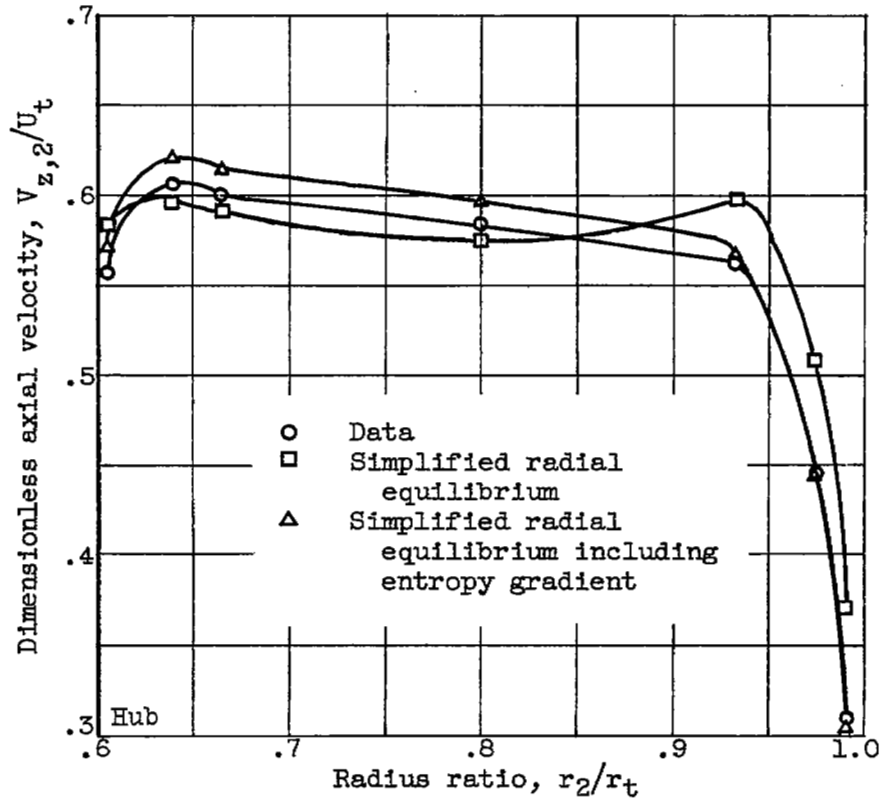


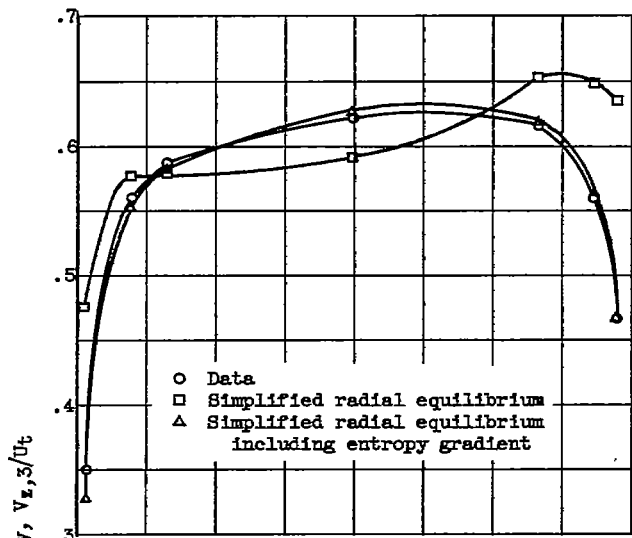
Figure 22. - Simplified-radial-equilibrium axial-velocity comparison after rotor for single-stage transonic compressor. Boundary-layer investigation for configuration of reference 10 for rotor plus stators; zero inlet whirl; rotor-inlet hub-tip ratio, 0.53; rotor-blade aspect ratio, 1.3.



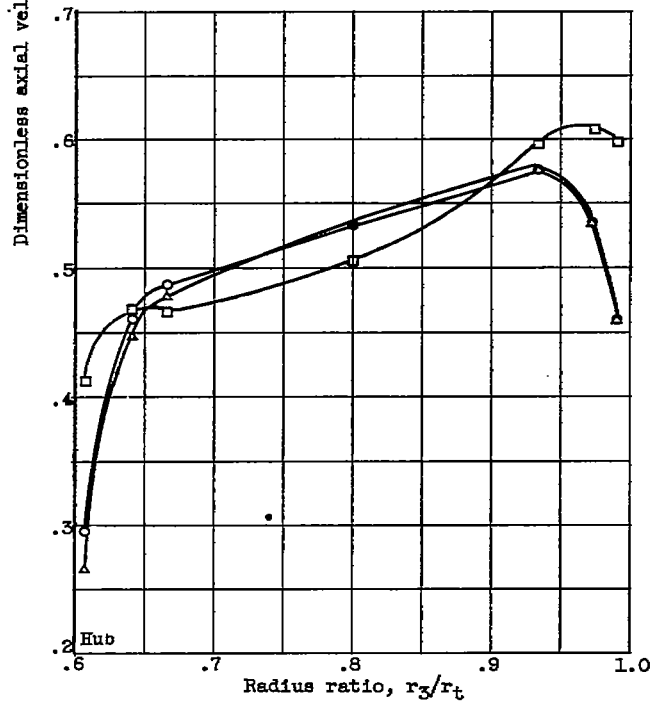
(c) Low flow ϕ_1 , 0.484; 60 percent design speed.

Figure 22. - Concluded. Simplified-radial-equilibrium axial-velocity comparison after rotor for single-stage transonic compressor. Boundary-layer investigation for configuration of reference 10 for rotor plus stators: zero inlet whirl; rotor-inlet hub-tip ratio, 0.53; rotor-blade aspect ratio, 1.3.

3038



(a) High flow $\phi_1, 0.481$.



(b) Peak efficiency point $\phi_1, 0.460$.

Figure 23. - Simplified-radial-equilibrium axial-velocity comparison after stators for single-stage compressor. Boundary-layer investigation for configuration of reference 10 for rotor plus stators: rotor-inlet hub-tip ratio, 0.53; stator-blade aspect ratio, 1.2; 100 percent design speed.

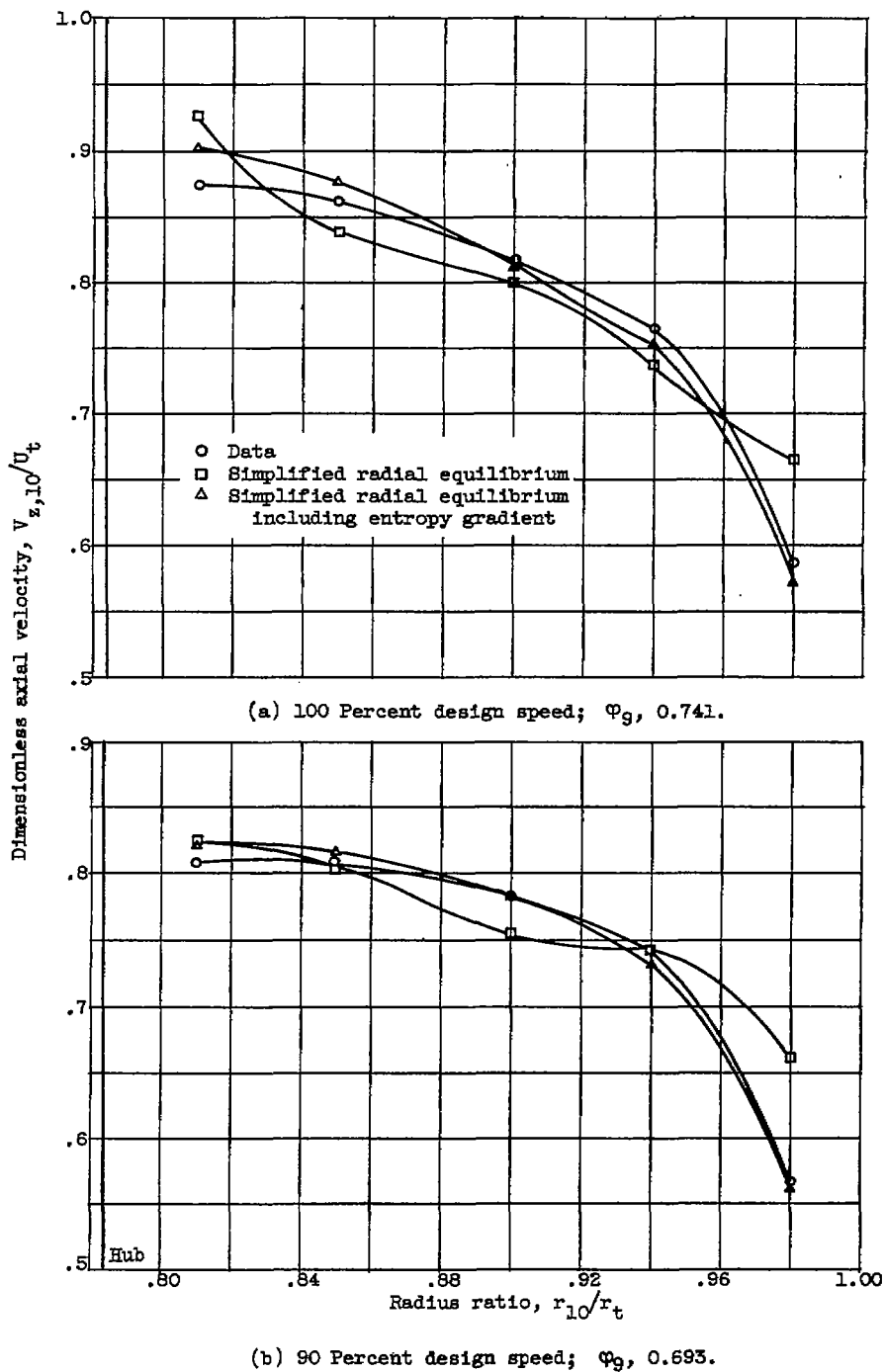


Figure 24. - Simplified-radial-equilibrium axial-velocity comparison after fifth rotor of 10-stage compressor. Multistage investigation for configuration of reference 6: wheel-minus-vortex inlet whirl; rotor-inlet hub-tip ratio, 0.76; rotor-blade aspect ratio, 1.7.

3038.

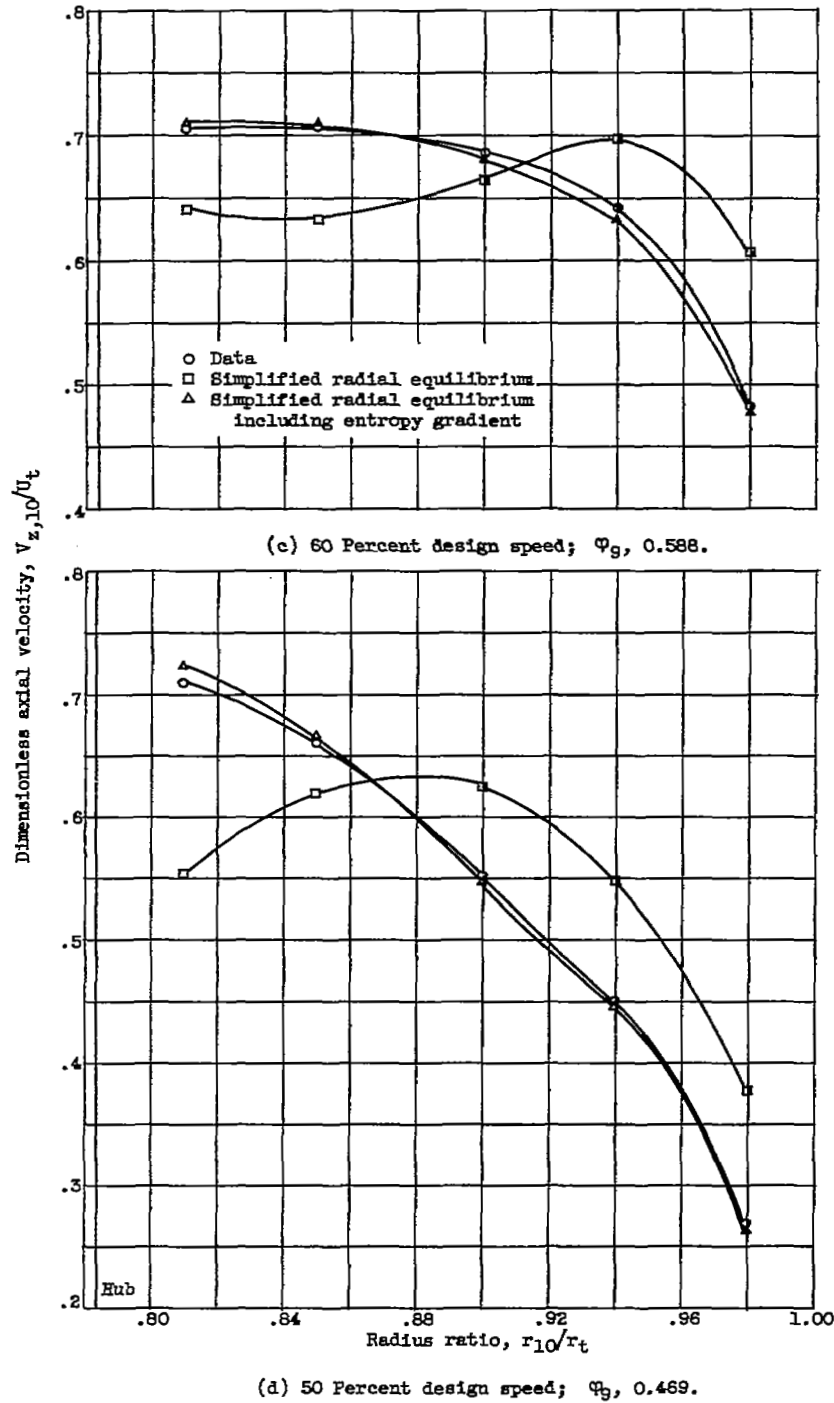
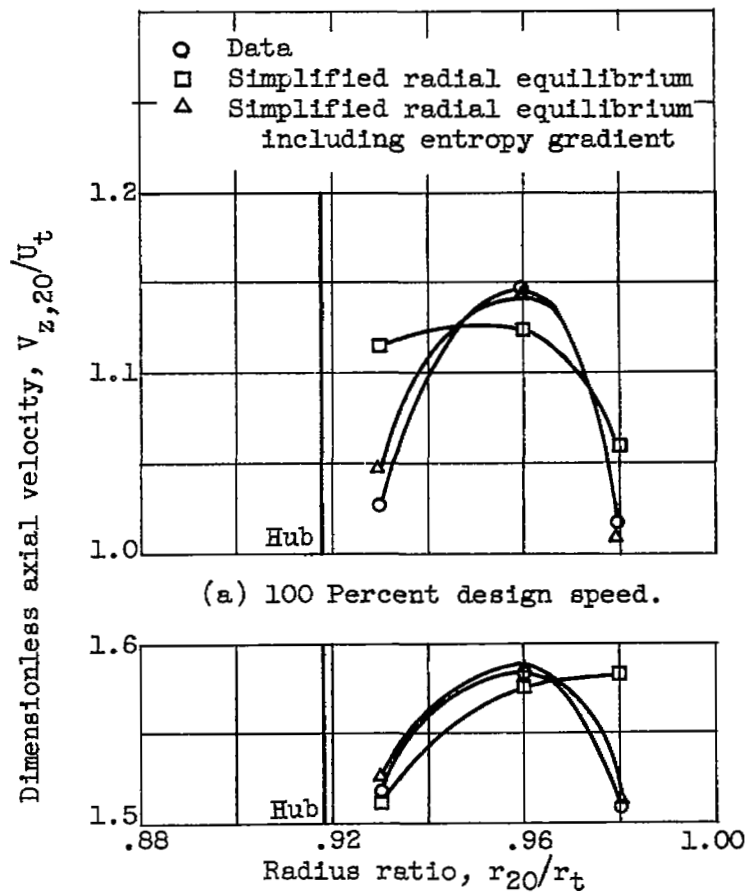


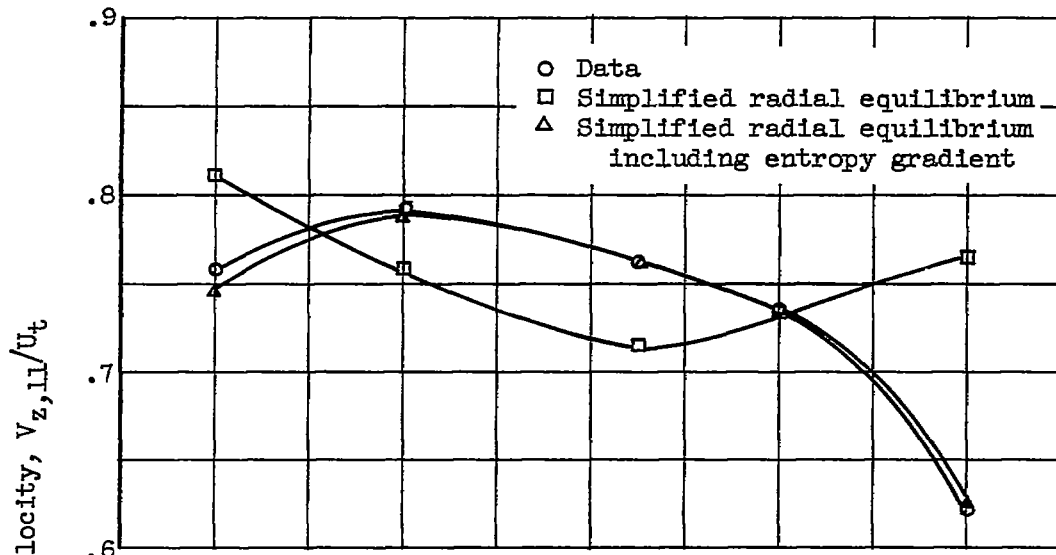
Figure 24. - Concluded. Simplified-radial-equilibrium axial-velocity comparison after fifth rotor of 10-stage compressor. Multistage investigation for configuration of reference 6; wheel-minus-vortex inlet whirl; rotor-inlet hub-tip ratio, 0.76; rotor-blade aspect ratio, 1.7.



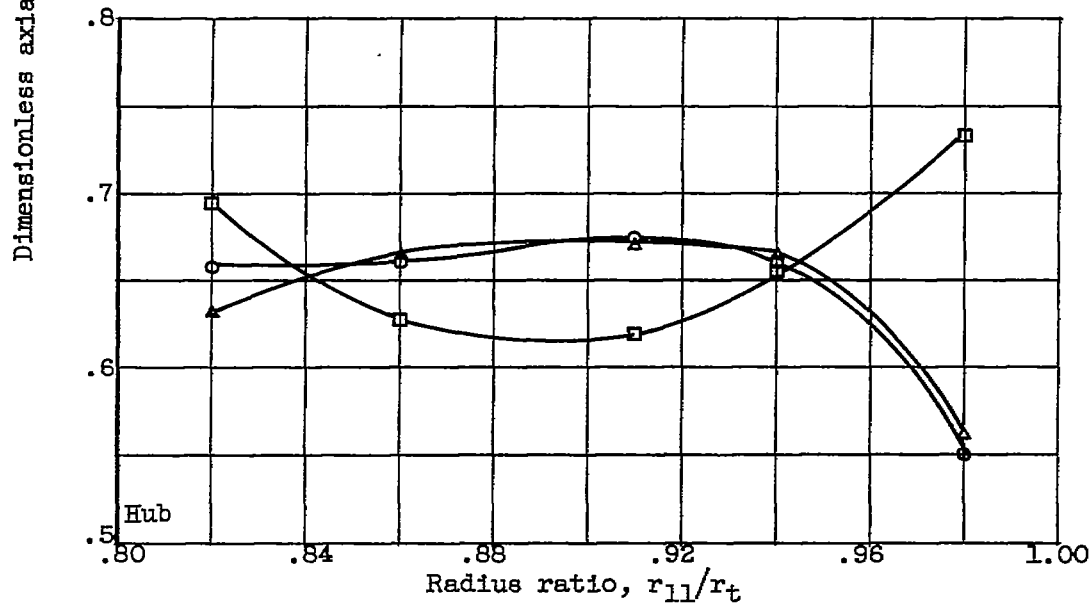
(a) 100 Percent design speed.

(b) 50 Percent design speed.

Figure 25. - Simplified-radial-equilibrium axial-velocity comparison after tenth rotor of 10-stage compressor. Multistage investigation for configuration of reference 6: wheel-minus-vortex inlet whirl; rotor-inlet hub-tip ratio, 0.91; rotor-blade aspect ratio, 0.82.

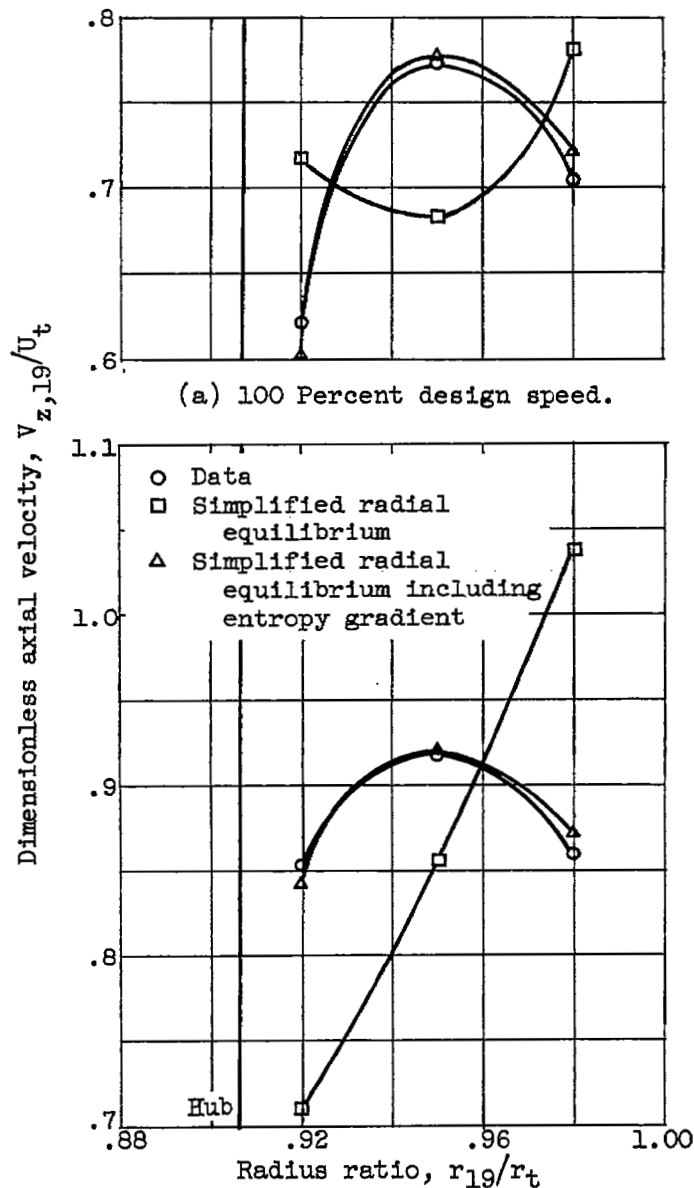


(a) Peak efficiency point $\Phi_9, 0.689$.



(b) Low flow $\Phi_9, 0.606$.

Figure 26. - Simplified-radial-equilibrium axial-velocity comparison after fifth stator of 10-stage compressor. Multistage investigation for configuration of reference 6: wheel-minus-vortex inlet whirl; rotor-inlet hub-tip ratio, 0.76; stator-blade aspect ratio, 1.6; 100 percent design speed.



(b) 50 Percent design speed.

Figure 27. - Simplified-radial-equilibrium axial-velocity comparison after ninth stator of 10-stage compressor. Multistage investigation for configuration of reference 6: wheel-type inlet-whirl; rotor-inlet hub-tip ratio, 0.89; stator-blade aspect ratio, 0.87.

NASA Technical Library



3 1176 01435 3438

CONFIDENTIAL